AGU PUBLICATIONS

Reviews of Geophysics

RESEARCH ARTICLE
10.1002/2014RG000455

Key Points:
- Ensemble average cross correlation not exactly = Green's function
- Relationship between Green's function/noise data depends on experimental setup
- We provide a pedagogical review of ambient noise theory with simple examples

Correspondence to:
L. Boschi,
lapo.boschi@upmc.fr

Citation:
Boschi, L., and C. Weemstra (2015), Stationary-phase integrals in the cross correlation of ambient noise, *Rev. Geophys.*, *53*, doi:10.1002/2014RG000455.

Received 3 APR 2014
Accepted 30 APR 2015
Accepted article online 14 MAY 2015

©2015. American Geophysical Union. All Rights Reserved.

Stationary-phase integrals in the cross correlation of ambient noise

Lapo Boschi[1,2] and Cornelis Weemstra[3]

[1] Institut des Sciences de la Terre Paris, Sorbonne Universités, Pierre and Marie Curie University Paris 06, UMR 7193, Paris, France, [2] Institut des Sciences de la Terre Paris, CNRS, UMR 7193, Paris, France, [3] Department of Geoscience and Engineering, Delft University of Technology, Delft, Netherlands

Abstract The cross correlation of ambient signal allows seismologists to collect data even in the absence of seismic events. "Seismic interferometry" shows that the cross correlation of simultaneous recordings of a random wavefield made at two locations is formally related to the impulse response between those locations. This idea has found many applications in seismology, as a growing number of dense seismic networks become available: cross-correlating long seismic records, the Green's function between instrument pairs is "reconstructed" and used, just like the seismic recording of an explosion, in tomography, monitoring, etc. These applications have been accompanied by theoretical investigations of the relationship between noise cross correlation and the Green's function; numerous formulations of "ambient noise" theory have emerged, each based on different hypotheses and/or analytical approaches. The purpose of this study is to present most of those approaches together, providing a comprehensive overview of the theory. Understanding the specific hypotheses behind each Green's function recipe is critical to its correct application. Hoping to guide nonspecialists who approach ambient noise theory for the first time, we treat the simplest formulation (the stationary-phase approximation applied to smooth unbounded media) in detail. We then move on to more general treatments, illustrating that the "stationary-phase" and "reciprocity theorem" approaches lead to the same formulae when applied to the same scenario. We show that a formal cross correlation/Green's function relationship can be found in complex, bounded media and for nonuniform source distributions. We finally provide the bases for understanding how the Green's function is reconstructed in the presence of scattering obstacles.

1. Introduction

In "seismic interferometry," the Green's function, or impulse response, of a medium can be determined empirically, based on the background signal recorded by two instruments over some time. The term "Green's function," ubiquitous in ambient noise literature, indicates the response of a medium to an impulsive excitation: a point source [e.g., *Morse and Ingard*, 1986; *Aki and Richards*, 2002]. Measuring a Green's function amounts to recording the ground oscillations that follow an explosion: exploiting the "ambient noise," the same signal can be measured without setting off any explosive. This approach was foreshadowed by several early studies in ocean acoustics [e.g., *Eckart*, 1953; *Cox*, 1973] and small-scale seismology [*Aki*, 1957; *Claerbout*, 1968] and later applied successfully to helioseismology [*Duvall et al.*, 1993; *Woodard*, 1997], ultrasound [*Weaver and Lobkis*, 2002; *Malcolm et al.*, 2004], terrestrial seismology [*Campillo and Paul*, 2003; *Shapiro et al.*, 2005], infrasound [*Haney*, 2009], and engineering [*Snieder and Şafak*, 2006; *Kohler et al.*, 2007].

Ambient noise seismology on Earth takes advantage of the "ambient," low-energy signal that seems to be generated continuously by the coupling between oceans and solid Earth [e.g., *Longuet-Higgins*, 1950; *Hasselmann*, 1963; *Stehly et al.*, 2006; *Kedar et al.*, 2008; *Hillers et al.*, 2012; *Gualtieri et al.*, 2013; *Traer and Gerstoft*, 2014]. Its resolution is not limited by the nonuniform distribution of earthquakes or by the difficulties inherent in setting up a man-made seismic source. Most ambient energy pertains to surface waves of period between ~5 s and ~30 s, which are difficult to observe in the near field of an earthquake, and almost completely attenuated in the far field, where only longer-period surface waves can be measured. Ambient noise-based surface-wave observations in this frequency range are thus complementary to traditional observations and particularly useful to map the crust, lithosphere, and asthenosphere: the shorter the surface-wave period, the shallower the depth range. Some recent studies [*Ruigrok et al.*, 2011; *Ito and Shiomi*, 2012; *Poli et al.*, 2012a, 2012b; *Gorbatov et al.*, 2013; *Nishida*, 2013] show that not only surface waves but also body waves traveling

over large distances and/or reflected by Earth discontinuities (the Moho, the upper-to-lower mantle boundary, etc.) can be extracted from ambient signal cross correlations.

Ambient noise correlation allows one to build a seismic data set even in the absence of earthquakes. In practice, the Green's function is reconstructed only approximately and within a limited frequency band, but that is enough to estimate relevant parameters such as group and phase velocity of surface waves. This is valuable for a number of different applications, allowing passive imaging at the reservoir scale and in the context of hydrocarbon industry [*De Ridder and Dellinger*, 2011; *Corciulo et al.*, 2012; *Weemstra et al.*, 2013] as well as monitoring of time-dependent changes in material properties around an active fault [*Wegler and Sens-Schonfelder*, 2007], in the rigidity of a landslide-prone area [*Mainsant et al.*, 2012] or in the shape and location of magma [*Brenguier et al.*, 2011] and hydrocarbon [*De Ridder et al.*, 2014] reservoirs.

The last decade has seen the publication of a number of increasingly exhaustive mathematical descriptions of the phenomenon of Green's function reconstruction from ambient recordings [*Lobkis and Weaver*, 2001; *Derode et al.*, 2003; *Snieder*, 2004; *Wapenaar*, 2004; *Weaver and Lobkis*, 2004; *Roux et al.*, 2005; *Wapenaar et al.*, 2005; *Nakahara*, 2006; *Sanchez-Sesma and Campillo*, 2006; *Wapenaar et al.*, 2006; *Tsai*, 2009; *Weaver et al.*, 2009]. In general, a mathematical relationship is found between the Green's function associated with the locations of two receivers (i.e., the response, observed at one of the receivers, to a point source deployed at the other receiver) and the cross correlation [e.g., *Smith*, 2011], computed over a long time interval, between the random ambient signal recorded by the receivers. (A detailed account of how ambient data are treated is given by *Bensen et al.* [2007].) Different approaches to establishing this relationship have been followed, however, resulting in different formulations. Most authors first develop the theory for the simple case of acoustic (scalar) wave propagation in two- or three-dimensional media. Some formulations hold for heterogeneous and/or bounded media, while others are limited to infinite homogeneous media. Defining ambient noise (a "diffuse field") mathematically is a nontrivial problem per se: some authors describe it as the superposition of plane waves propagating in all directions; others prefer to superpose impulsive responses (Green's functions), sometimes in two dimensions, sometimes in three; others yet define the noise field as one where all normal modes have the same probability of being excited. Finally, the expression Green's function itself is ambiguous: in elastodynamics, it may refer to the response of a medium to an impulsive force, impulsive stress, or impulsive initial conditions in displacement, or velocity. While specialists are well aware of these differences and their implications, interferometry "users" (including the authors of this article) are sometimes confused as to the theoretical basis, and practical reliability, of the methods they apply.

The goal of this study is to show in detail how several different derivations of "ambient noise theory" lead to apparently different but indeed perfectly coherent results. We first treat some particularly simple scenarios: ambient noise in a homogeneous lossless (i.e., nonattenuating) 2-D or 3-D medium, generated by azimuthally uniform, 2-D or 3-D distributions of point sources, or by plane waves propagating in all directions. The analogy between acoustic waves in two dimensions and Rayleigh waves is discussed. Analytical expressions for the cross correlation of ambient signals in all these physical settings are given in section 3 and implemented numerically in section 4. In all the simple cases we consider, the cross correlation of ambient signal as derived in section 3 coincides with the integral, over the area occupied by sources, of an overall very oscillatory function, which becomes slowly varying only around a small set of so-called "stationary" points. We show in section 5 how such integrals are solved via the approximate "stationary-phase" method (Appendix A); different analytical relationships between cross correlation and Green's function are thus found and discussed; they are later summarized in section 9. In section 8 we apply, again, the stationary-phase method to a more complicated medium including one scattering obstacle, which allows us to introduce the concept, often found in ambient noise literature, of "spurious" arrival in cross correlation. Finally, the so-called "reciprocity theorem" approach provides an analytical relationship between Green's function and cross correlation that is valid in arbitrarily complex, attenuating media. We describe it in detail in section 6, together with a few other "alternative" approaches to ambient noise theory; the consistency between reciprocity theorem and stationary-phase results is verified. To avoid ambiguity as much as possible, we provide an overview of the underlying theory for both acoustics and elastodynamics in section 2 and a derivation of acoustic Green's functions in Appendix E. By collecting all this previously scattered material in a single review, we hope to provide a useful tool for graduate students and nonspecialists approaching the theory of acoustic and seismic ambient noise for the first time. Most of the results presented here are limited to nonscattering, nondissipative, homogeneous acoustic media and to surface wave (and not body wave) propagation in elastic media. These simplifications have the advantage of allowing a self-contained, relatively uncluttered derivation. We explore more realistic setups

(nonuniform source distributions; scattering) in sections 7 and 8. The thorough understanding of ambient noise cross correlation in simple media will serve as a solid platform for more advanced investigations. Readers that are mostly interested in applications to realistic environments are referred to the differently minded reviews of *Curtis et al.* [2006], *Larose et al.* [2006], *Gouedard et al.* [2008], *Wapenaar et al.* [2010a, 2010b], *Snieder and Larose* [2013], *Ritzwoller* [2014], and *Campillo and Roux* [2014].

2. Governing Equations

In this study, analytical relationships between Green's functions and the cross correlation of ambient signal are derived in a number of different scenarios: spherical acoustic waves in two and three dimensions, Rayleigh waves, and plane waves. We first summarize the theory underlying each of these cases.

2.1. Acoustic Waves From a Point Source in Free Space

Pressure p in homogeneous, inviscid fluids occupying a three-dimensional space obeys the linear, lossless wave equation

$$\nabla^2 p - \frac{1}{c^2}\frac{\partial^2 p}{\partial t^2} = \frac{\partial q}{\partial t}, \tag{1}$$

where ∇ is the gradient operator, c^2 the ratio of adiabatic bulk modulus to density, t denotes time, and the forcing term q is the (apparent) mass production per unit volume per unit time, representing, e.g., an explosion or a loudspeaker [e.g., *Kinsler et al.*, 1999, chap. 5].

If $\partial q/\partial t = \delta(\mathbf{r}-\mathbf{r_0})\delta(t-t_0)$, with δ the Dirac distribution, $\mathbf{r}$ the position vector, and $\mathbf{r_0}$, t_0 the location and time of an impulsive sound source, respectively, equation (1) is referred to as "Green's problem" and its solution for p as Green's function. Once the Green's problem is solved, the response of the system to however complicated a source is found by convolving the Green's and source functions [e.g., *Morse and Ingard*, 1986; *Aki and Richards*, 2002]. The Green's function G_{3D} associated with (1) is derived in Appendix E here, equations (E21) and (E22), working in spherical coordinates and choosing (without loss of generality) $t_0 = 0$ and $\mathbf{r}_0 = \mathbf{0}$.

2.2. Membrane Waves From a Point Source

Equation (1) also describes the motion of an elastic membrane. In this case, p can be interpreted as displacement in the vertical direction (for a horizontal membrane), ∇ is the surface gradient, and c the ratio of the membrane tension per unit length to its surface density [e.g., *Kinsler et al.*, 1999, section 4.2]. The associated Green's function G_{2D} is determined analytically in Appendix E, equations (E15) and (E16).

2.3. Rayleigh Waves From a Point Source

The "potential" representation of surface wave propagation, adopted, e.g., by *Tanimoto* [1990], consists of writing Rayleigh wave displacement

$$\mathbf{u}_R = U(z)\,\hat{\mathbf{z}}\,\Psi_R(x,y;t) + V(z)\nabla_1\Psi_R(x,y;t), \tag{2}$$

where x, y, and z are Cartesian coordinates (z denotes depth), the "vertical eigenfunctions" U and V depend on z only, and the Rayleigh wave potential Ψ_R varies only laterally (but varies with time). $\hat{\mathbf{x}}$, $\hat{\mathbf{y}}$, and $\hat{\mathbf{z}}$ are unit vectors in the directions of the corresponding coordinates, and the operator $\nabla_1 = \hat{\mathbf{x}}\frac{\partial}{\partial x} + \hat{\mathbf{y}}\frac{\partial}{\partial y}$. Love wave displacement is accordingly written

$$\mathbf{u}_L = -W(z)\hat{\mathbf{z}} \times \nabla_1\Psi_L(x,y;t), \tag{3}$$

with $\times$ denoting a vector product.

Substituting the *Ansätze* (2) and (3) into the 3-D equation of motion, one finds that both potentials Ψ_R and Ψ_L satisfy

$$\nabla_1^2\Psi_{R,L} - \frac{1}{c_{R,L}^2}\frac{\partial^2\Psi_{R,L}}{\partial t^2} = T_{R,L}, \tag{4}$$

i.e., equation (1), with $c_{R,L}$ denoting phase velocity and T_R, T_L scalar forcing terms [e.g., *Tanimoto*, 1990; *Tromp and Dahlen*, 1993; *Udías*, 1999].

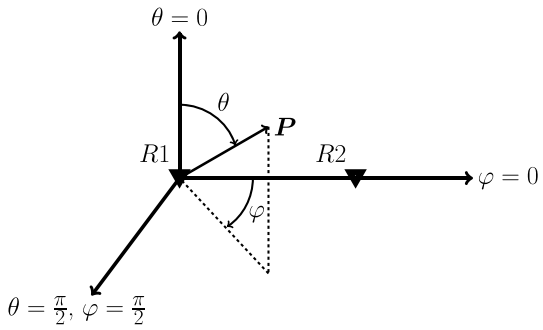

Figure 1. Spherical reference frame used throughout this study. The origin is placed at the location of receiver 1 (*R*1), while receiver 2 (*R*2) lies on the $\varphi = 0$, $\theta = \pi/2$ axis. The distance between the origin and a point *P* is denoted *r*.

The Green's problem associated with (4) coincides with the 2-D, membrane wave problem of section 2.2 and Appendix E, and the Green's function corresponding to $\Psi_{R,L}$ is, again, G_{2D} of equations (E15) and (E16). The surface wave Green's function can be obtained from the scalar Green's function G_{2D} via equation (2) [*Tromp and Dahlen*, 1993, section 5].

Importantly, according to (2), the vertical component of Rayleigh wave displacement $\mathbf{u}_R$ is simply $U(z)\Psi_R(x, y; t)$; $U(z)$ is a function of z that does not change with time so that the *phase* of the vertical component of $\mathbf{u}_R$ coincides with that of the potential $\Psi_R(x, y; t)$. The analysis of 2-D ambient noise that we conduct here holds therefore for Rayleigh waves propagating in a 3-D medium (in the Earth) and measured on the vertical component of seismograms, as far as the phase is concerned; amplitude needs to be scaled.

The Rayleigh-wave derivation of *Snieder* [2004] is also based on this idea, although in that study the separation between x, y, t dependence and z dependence follows from a normal-mode formulation [e.g., *Snieder*, 1986]. *Halliday and Curtis* [2008] explore the effects of subsurface sources, or lack thereof, on Green's function reconstruction; their results are consistent with ours and with those of *Snieder* [2004] whenever their setup is the same as ours, i.e., uniform source distribution over the Earth's (laterally invariant) surface.

2.4. Plane Waves

Some authors [e.g., *Aki*, 1957; *Sanchez-Sesma and Campillo*, 2006; *Tsai*, 2009; *Boschi et al.*, 2013] have studied diffuse wavefields with cylindrical symmetry, which they described as the superposition of plane waves (rather than spherical or circular as seen so far in this article) traveling along many different azimuths. If its right-hand side $\frac{\partial q}{\partial t} = 0$, equation (1) is satisfied by a monochromatic plane wave

$$p(\mathbf{r}, t) = S(\omega)\cos(\omega t + \mathbf{k}\cdot\mathbf{r}), \tag{5}$$

where the vector $\mathbf{k}$ is constant and defines the direction of propagation, and the amplitude function $S(\omega)$ is arbitrary. A plane wave approximates well the response of a medium to a real source, at receivers that are sufficiently far from the source.

3. Cross Correlation in a Diffuse Wavefield

We are interested in the cross correlation between recordings of a *diffuse* wavefield made at a pair of receivers. In acoustics, a diffuse wavefield is such that the energy associated with propagating waves is the same at all azimuths of propagation [e.g., *Kinsler et al.*, 1999, section 12.1]. (The expression "equipartitioned field," often intended as a synonym of "diffuse," is used in the literature with slightly different meanings depending on the context [*Snieder et al.*, 2010], and we chose not to employ it here to avoid ambiguity.) While ambient noise recorded on Earth is not strictly diffuse [*Mulargia*, 2012], diffuse field theory successfully describes many seismic observations, and as such it is at least a useful first approximation of real ambient noise.

We simulate an approximately diffuse wavefield by averaging (or, in seismology jargon, "stacking") cross correlations associated with sources distributed uniformly over a circle or a sphere surrounding the receivers. This is equivalent to the source azimuth being random; i.e., over time, all azimuths are sampled with equal frequency/probability.

We center our spherical reference frame at the location of "receiver 1" (*R*1) and orient it so that "receiver 2" (*R*2) lies on the $\varphi = 0$, $\theta = \pi/2$ axis (Figure 1). We choose sources to be separated in time, that is to say, a receiver never records signal from more than one source at the same time: while diffuse wavefields in the real world might result from multiple, simultaneous sources, our simplification is justified by the mathematical finding that the so-called "cross terms", i.e., the receiver-receiver cross correlation of signal generated by different sources, are negligible when "ensemble averaged." A proof is given, e.g., by *Weemstra et al.* [2014] and is summarized here in Appendix D.

Let us call S a source location and r_{iS} the distance between S and the ith receiver. If the source at S is an impulsive point source, the recorded signals coincide with the Green's function associated with the source location S, evaluated at $R1$ and $R2$. In 3-D, the Green's function is given by equation (E22), and in the frequency domain the cross correlation reads

$$G_{3D}(r_{1S},\omega)\,G^{*}_{3D}(r_{2S},\omega)=\frac{1}{(4\pi c)^2}\frac{1}{2\pi}\frac{e^{i\frac{\omega}{c}(r_{2S}-r_{1S})}}{r_{1S}\,r_{2S}} \tag{6}$$

(here and in the following the superscript $*$ denotes complex conjugation). Since the dimension of G_{3D} in the frequency domain is time over squared distance (Appendix E), that of equation (6) is squared time over distance to the power of 4 (or time over distance to the power of 4 in the time domain).

In 2-D (membrane waves and Rayleigh waves), G_{2D} is given by (E16), and the cross correlation

$$G_{2D}(r_{1S},\omega)\,G^{*}_{2D}(r_{2S},\omega)=\frac{-i}{32\pi c^4}H_0^{(2)}\left(\frac{\omega r_{1S}}{c}\right)\left[-iH_0^{(2)}\left(\frac{\omega r_{2S}}{c}\right)\right]^{*}. \tag{7}$$

The cumulative effect of multiple sources S is obtained by rewriting expression (6) or (7) for each S, with r_{1S} and r_{2S} varying as functions of the distance r and azimuth φ (and, in 3-D, inclination θ) of S with respect to the origin and summing.

We shall consider several different scenarios:

(i) In 3-D space, for a continuous distribution of sources along a circle in the $\theta=\pi/2$ plane (centered, for the sake of simplicity, at $R1$) summing the cross correlations over S leads to an integral over φ,

$$I_C(\omega)=\frac{1}{(4\pi c)^2}\frac{1}{4\pi^2}\int_{-\pi}^{\pi}d\varphi\,n_C(\varphi)\frac{e^{i\frac{\omega}{c}(r_{2S}(\varphi)-r_{1S}(\varphi))}}{r_{1S}(\varphi)\,r_{2S}(\varphi)}, \tag{8}$$

with n_C the number of sources per unit azimuth or source density.

(ii) If sources are distributed on a sphere centered at $R1$, the double integral is over the surface of the sphere (4π solid radians), and

$$\begin{aligned}I_S(\omega)&=\frac{1}{4\pi}\int_0^{\pi}d\theta\sin\theta\int_{-\pi}^{\pi}d\varphi\,n_S(\theta,\varphi)\,G_{3D}(r_{1S},\omega)\,G^{*}_{3D}(r_{2S},\omega)\\&=\frac{1}{4\pi}\frac{1}{(4\pi c)^2}\frac{1}{2\pi}\int_0^{\pi}d\theta\sin\theta\int_{-\pi}^{\pi}d\varphi\,n_S(\theta,\varphi)\frac{e^{i\frac{\omega}{c}(r_{2S}(\theta,\varphi)-r_{1S}(\theta,\varphi))}}{r_{1S}(\theta,\varphi)\,r_{2S}(\theta,\varphi)},\end{aligned} \tag{9}$$

where n_S denotes the number of sources per unit of solid angle on the sphere.

(iii) Switching to 2-D, i.e., to Rayleigh waves or elastic waves propagating on a membrane, we need to integrate expression (7) over the position occupied by S. Assuming a source distribution analogous to that of case (i), with sources along a circle, and source density n_M a function of φ only, we find after some algebra that cross correlation is described by

$$\begin{aligned}I_{MW}(\omega)&=\frac{1}{32\pi c^4}\frac{1}{2\pi}\int_{-\pi}^{\pi}d\varphi\,n_M(\varphi)\,H_0^{(2)}\left(\frac{\omega r_{1S}(\varphi)}{c}\right)H_0^{(2)*}\left(\frac{\omega r_{2S}(\varphi)}{c}\right)\\&\approx\frac{1}{16\pi^2c^3}\frac{1}{2\pi}\int_{-\pi}^{\pi}d\varphi\,n_M(\varphi)\frac{e^{i\frac{\omega}{c}(r_{1S}(\varphi)-r_{2S}(\varphi))}}{\omega\sqrt{r_{1S}(\varphi)r_{2S}(\varphi)}},\end{aligned} \tag{10}$$

where we have replaced the Hankel function $H_0^{(2)}$ with its asymptotic (high-frequency and/or far-field) approximation, equation (9.2.4) of *Abramowitz and Stegun* [1964]; this approximation is necessary to later solve the integral in (10) via the stationary-phase method. Notice that we do not yet require the wavefield to be isotropic: at this point n_C, n_S, and n_M are arbitrary functions of θ and φ. We will show in section 5, however, that they need to be smooth or constant for the stationary-phase approximation to be applicable.

(iv) In the plane wave approach of section 2.4 no source location is specified, but one combines plane waves (5) traveling along all azimuths φ. At $R1$, the monochromatic plane wave of frequency ω_0 traveling in the direction φ is

$$p(R1,t)=S(\omega_0)\cos(\omega_0 t); \tag{11}$$

at $R2$ the same signal is recorded at a different time, and

$$p(R2,t)=S(\omega_0)\cos\left[\omega_0\left(t+\frac{\Delta\cos\varphi}{c}\right)\right]. \tag{12}$$

Based on equations (11) and (12), *Boschi et al.* [2013] show that the source-averaged, two-station cross correlation of monochromatic plane waves at frequency ω_0 can be written

$$I_{PW}(\omega_0, t) = \frac{q(\omega_0)}{2\pi} \int_0^\pi \mathrm{d}\varphi \cos\left[\omega_0 \left(t + \frac{\Delta \cos\varphi}{c}\right)\right], \tag{13}$$

obtained from equations (18) and (21) of *Boschi et al.* [2013] through the change of variable $t_d = \Delta\cos(\varphi)/c$ and assuming source density and the amplitude term $q(\omega)$ (reflecting the frequency spectrum of the source) to be constant with respect to φ. The Fourier transform of (13) is

$$I_{PW}(\omega_0, \omega) = \frac{q(\omega_0)}{\sqrt{8\pi}} \int_0^\pi \mathrm{d}\varphi \left[\delta(\omega + \omega_0) + \delta(\omega - \omega_0)\right] \mathrm{e}^{\mathrm{i}\omega \frac{\Delta \cos\varphi}{c}}. \tag{14}$$

Equation (14) is valid for any ω_0; using the properties of the Dirac δ function, we generalize it to

$$I_{PW}(\omega) = \frac{q(\omega)}{\sqrt{2\pi}} \int_0^\pi \mathrm{d}\varphi \cos\left(\omega \frac{\Delta \cos\varphi}{c}\right). \tag{15}$$

We integrate equations (8)–(10) and (15) numerically in section 4; this exercise will serve to validate the results, illustrated in section 5, of integrating the same equations analytically via the stationary-phase approximation.

The case of a spatially (and not just azimuthally) uniform distribution of sources over a plane or the 3-D space is not treated here in the interest of brevity. It essentially requires that expression (8), (9), or (10) be additionally integrated over source location; in practice, one needs to integrate over the *distance* between source and origin, along the azimuths of stationary points only (one-dimensional integrals) [*Snieder*, 2004; *Sato*, 2010].

4. Numerical Integration

Before deriving approximate analytical solutions for the integrals in equations (8)–(10) and (15), we implement these equations numerically. In practice, we evaluate equations (E16) and (E22) at $R1$, $R2$, to determine G_{2D} or G_{3D} numerically for discrete sets of sources and values of ω. For each source, we cross correlate the Green's function calculated at $R1$ with that calculated at $R2$. We stack the resulting cross correlations in the time domain, which is equivalent to calculating the φ and θ integrals in the equations above. The stacks can be compared with predictions based on the analytical formulae that we shall illustrate below.

4.1. Ring of Sources

The setup associated with equation (8) is implemented numerically, placing 720 equally spaced sources along the planar ring centered at $R1$. $R1$ and $R2$ are 20 km away from one another, and wave speed is 2 km/s. We implement equation (8) directly at frequencies between $\pm$10 Hz, with sampling rate 20 Hz; we taper the highest and lowest frequencies to avoid ringing artifacts and inverse Fourier transform via numerical fast Fourier transform [*Cooley and Tukey*, 1965]. The corresponding cross correlations are shown in the "gather" plot of Figure 2a. Sources aligned with the two receivers (azimuth 0° or 180°) result in the longest delay time between arrival of the impulse at $R1$ and $R2$: cross correlation is nonzero near $\pm$10 s, which corresponds to the propagation time between $R1$ and $R2$. Sources at azimuth around ~90° and ~270° are approximately equidistant from $R1$ and $R2$, resulting in the impulse hitting $R1$ and $R2$ simultaneously, and cross correlation in Figure 2a being nonzero at ~0 s for those source azimuths. The result of averaging over all sources is shown in Figure 2b. It is clear that the imaginary part of the time domain signal is 0, as it should be. As for the real part, cross correlations associated with sources at azimuth 0° or 180° add up constructively; the cumulative contribution of other sources is smaller but nonnegligible. The source-averaged cross correlation is accordingly dominated by two peaks corresponding to energy traveling in a straight path from $R2$ to $R1$ (generated by sources at azimuth 0°) and from $R1$ to $R2$ (sources at 180°). The two peaks are often labeled "causal" and (not quite appropriately) "anticausal" (or "acausal"), respectively. In this particular case, the causal and anticausal peaks have different amplitude. This asymmetry reflects the asymmetry in the locations of $R1$ and $R2$ with respect to the source distribution: $R2$ is closer to sources at $\varphi = 0°$ than $R1$ is to sources at $\varphi = 180°$, and waves hitting $R2$ have accordingly larger amplitude. The description of seismic/acoustic interferometry in terms of a stationary-phase integral (section 5.1 and Appendix A) explains mathematically why sources at 0° or 180° are most relevant and provides an analytical relationship between the source-averaged cross correlation in Figure 2b and the Green's function of the medium.

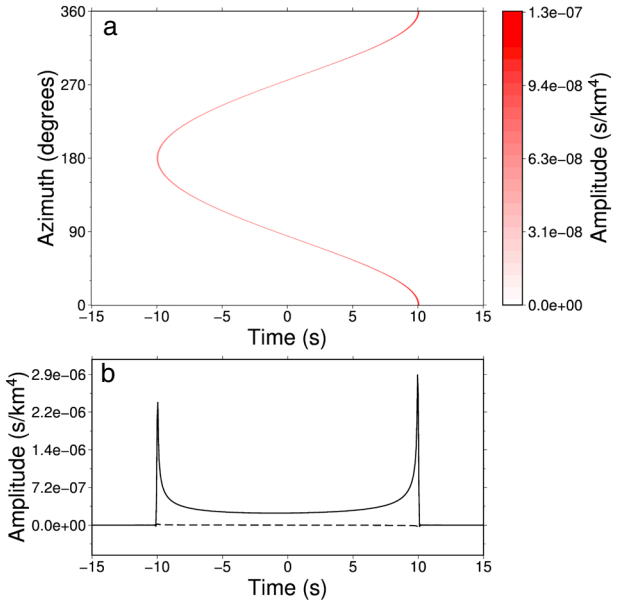

Figure 2. Cross correlations associated with a circular, planar distribution of sources surrounding the two receivers. $R1$ is at the center of a circle of sources with radius $R = 100$ km. $R2$ lies on the plane defined by $R1$ and the sources, $\Delta = 20$ km away from $R1$. Phase velocity $c = 2$ km/s. Source density $n_C(\varphi) = 2$ sources per degree, independent of φ. $G_{3D}(r_{1S}, \omega)$ and $G_{3D}(r_{2S}, \omega)$ are evaluated numerically and cross correlated for a ring of equally spaced sources. The result is inverse Fourier transformed and averaged over all sources. (a) Time-domain single-source cross correlations for all azimuths. (b) Real (solid line) and imaginary (dashed) parts of the source-averaged, time domain cross correlation, resulting from stacking the traces in Figure 2a. The dimension is that of $G_{3D}(\mathbf{r}, \omega)$, squared and integrated over frequency (inverse Fourier transformed).

4.2. Sources on a Sphere

We next distribute $\sim 10^3$ approximately equally spaced sources over the surface of a sphere of radius $R = 100$ km, centered at $R1$. $R2$ lies 20 km away from $R1$. In analogy with section 4.1, the signal recorded at $R1$ and that recorded at $R2$ (equation (E22)) are cross correlated for each source, and cross correlations are stacked, implementing equation (9). The source-averaged frequency-domain cross correlation is computed between ± 10 Hz, with sampling rate 20 Hz, and tapered at high frequency to avoid artifacts. The time-domain result is shown in Figure 3; in this case, no gather plot was made because of the difficulty of visualization when sources are distributed in three dimensions. The source-averaged cross correlation is real, as it should be; it is different from that of Figure 2b, in that cross correlations associated with sources at all azimuths add up constructively, resulting in a boxcar function. Again, the maximum delay time between arrival of the impulse at $R1$ and $R2$ (10 s in our setup) corresponds to sources at 0° and 180°, and no energy is recorded at $t > 10$ s; cross correlations are accordingly 0 at $t < -10$ s and $t > 10$ s. Despite the asymmetry in receiver location with respect to the sources, the stacked cross correlation is now symmetric. All these results are reproduced analytically in section 5.2.

4.3. Membrane Waves/Rayleigh Wave Potential

The setup associated with equation (10) is also reproduced numerically, placing 720 sources at 0.5° azimuth φ intervals along the ring centered at $R1$. Frequency varies between ± 10 Hz with sampling rate = 20 Hz; high frequencies are tapered as above. As we shall show analytically in section 5.3, equation (10) leads to a nonconvergent ω integral when a time domain expression for I_{MW} is sought; we therefore compute the time derivative of I_{MW} (multiplication by $i\omega$ in the frequency domain) before inverse Fourier transforming. In the interest of speed, we implement the asymptotic approximation of $H_0^{(2)}$ (i.e., the second line of equation (10)) rather than $H_0^{(2)}$ itself. The results are shown in Figure 4. The gather (Figure 4a) is qualitatively similar to that of Figure 2a, but Figure 4b shows that cross correlations associated with sources away from azimuth 0° and 180° cancel out when stacking. After stacking (Figure 4b) we verify that the time

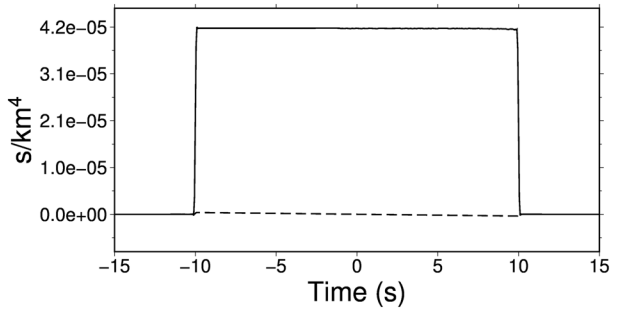

Figure 3. Real (solid line) and imaginary (dashed) parts of the average time domain cross correlation, resulting from stacking all cross correlations associated with a uniformly dense distribution of sources over a sphere. $R1$ is at the center of a sphere of sources with radius $R = 100$ km. $R2$ lies $\Delta = 20$ km away from $R1$. Phase velocity $c = 2$ km/s. The calculation is conducted numerically (section 4.2), by evaluating $G_{3D}(r_{1S}, \omega)$ and $G_{3D}(r_{2S}, \omega)$ for each source via equation (E22) and subsequently applying cross correlation, inverse Fourier transformation, and averaging over all sources.

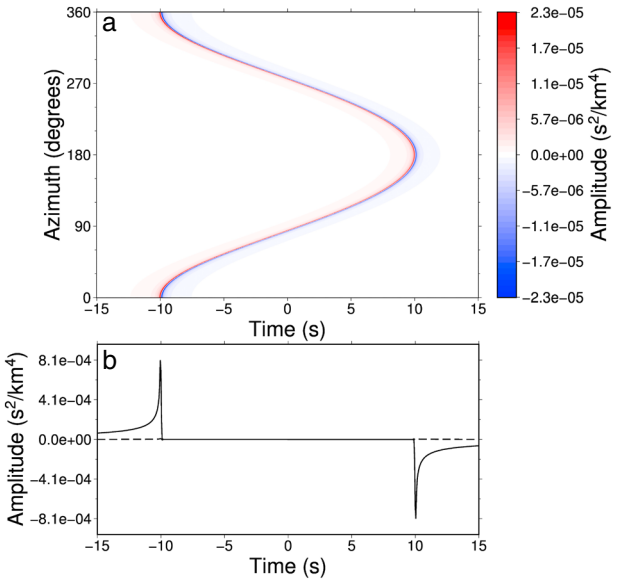

Figure 4. Cross correlations, differentiated with respect to time, associated with a circular, planar distribution of sources surrounding the two receivers in two dimensions, i.e., on a membrane. The setup is the same as in Figure 2. $G_{2D}(r_{1S},\omega)$ and $G_{2D}(r_{2S},\omega)$ are evaluated numerically and cross correlated for a ring of 720 equally spaced sources. The result is inverse Fourier transformed and averaged over all sources. (a) Time domain single-source cross correlations for all azimuths. (b) Real (solid line) and imaginary (dashed) parts of the stacked time derivative of the cross correlation, resulting from stacking the traces in Figure 4a.

derivative of I_{MW} is real. We also find that it is antisymmetric with respect to time, indicating that I_{MW} is symmetric, in agreement with the results of section 4.2 but not with section 4.1.

5. Analytical Formulae for Two Receiver Cross Correlations of a Diffuse Wavefield

As pointed out by *Snieder* [2004], integration with respect to θ and φ in equations (8)–(10) and (15) can also be conducted analytically by means of the stationary-phase approximation, the details of which are given in Appendix A. The numerical results of section 4 will serve as a reference to validate the approximate results presented below.

5.1. Ring of Sources in Free Space

The integrand at the right-hand side of equation (8) coincides with that in (A1), after replacing $\lambda=\omega$, $x=\varphi$ and defining $f(\varphi)=n_C(\varphi)/\left[4\pi^2 r_{1S}(\varphi) r_{2S}(\varphi)\right]$ and $\psi(\varphi)=\left[r_{1S}(\varphi)-r_{2S}(\varphi)\right]/c$. We shall first identify the values of φ such that $\psi'(\varphi)=0$ (stationary points), then use equation (A2) to evaluate the contribution of each stationary point to the integral, and finally combine them. Importantly, the stationary-phase approximation is valid at high frequencies $\omega \longrightarrow \infty$ (corresponding to $\lambda \longrightarrow \infty$ in section A1). Choosing the reference frame as described in section 3 (Figure 1), by definition r_{1S} is constant (we shall call it R) and, based on some simple geometrical considerations,

$$r_{2S}=\left[(R\cos\varphi-\Delta)^2+R^2\sin^2\varphi\right]^{\frac{1}{2}}=\left(R^2+\Delta^2-2\Delta R\cos\varphi\right)^{\frac{1}{2}}, \tag{16}$$

where Δ is interstation distance and $\Delta < R$ in our setup. It follows that

$$f(\varphi)=\frac{1}{(4\pi c)^2}\frac{n_C(\varphi)}{4\pi^2 R\left(R^2+\Delta^2-2\Delta R\cos\varphi\right)^{\frac{1}{2}}}, \tag{17}$$

$$\psi(\varphi)=\frac{1}{c}(r_{1S}-r_{2S})=\frac{1}{c}\left[\left(R^2+\Delta^2-2\Delta R\cos\varphi\right)^{\frac{1}{2}}-R\right], \tag{18}$$

and upon differentiating ψ with respect to φ,

$$\psi'(\varphi)=\frac{\Delta R\sin\varphi}{c\left(R^2+\Delta^2-2\Delta R\cos\varphi\right)^{\frac{1}{2}}}, \tag{19}$$

$$\psi''(\varphi)=\frac{\Delta R\cos\varphi}{c\left(R^2+\Delta^2-2\Delta R\cos\varphi\right)^{\frac{1}{2}}}-\frac{\Delta^2R^2\sin^2\varphi}{c\left(R^2+\Delta^2-2\Delta R\cos\varphi\right)^{\frac{3}{2}}}. \tag{20}$$

We infer from (19) that the stationary points of $\psi(\varphi)$ within the domain of integration are $\varphi=-\pi,0,\pi$ (corresponding to $\sin\varphi=0$). Following *Bender and Orszag* [1978], we rewrite equation (8) as a sum of integrals limited to the vicinity of stationary points and with a stationary point as one of the integration limits:

$$I_C(\omega)\approx\int_{-\pi}^{-\pi+\varepsilon}f(\varphi)e^{i\omega\psi(\varphi)}d\varphi+\int_{-\varepsilon}^{0}f(\varphi)e^{i\omega\psi(\varphi)}d\varphi+\int_{0}^{\varepsilon}f(\varphi)e^{i\omega\psi(\varphi)}d\varphi+\int_{\pi-\varepsilon}^{\pi}f(\varphi)e^{i\omega\psi(\varphi)}d\varphi, \tag{21}$$

which is valid for $\omega \longrightarrow \infty$ and arbitrarily small ε. Equation (A2) can now be used directly to integrate each of the terms at the right-hand side of (21), and after noticing that both $f(\varphi)$ and $\psi(\varphi)$ are symmetric with respect to $\varphi = 0$, we find

$$I_C(\omega) \approx 2f(\pi)\mathrm{e}^{\mathrm{i}\left(\omega\psi(\pi)\pm\frac{\pi}{4}\right)}\sqrt{\frac{\pi}{2\omega|\psi''(\pi)|}} + 2f(0)\mathrm{e}^{\mathrm{i}\left(\omega\psi(0)\pm\frac{\pi}{4}\right)}\sqrt{\frac{\pi}{2\omega|\psi''(0)|}}. \tag{22}$$

We now need to evaluate f, ψ, and ψ'' at 0 and π. It follows from the definition of f, from equations (18) and (20) and from the fact that $R > \Delta$ (and hence $|R - \Delta| = R - \Delta$) that

$$f(0) = \frac{1}{(4\pi c)^2}\frac{n_C(0)}{4\pi^2 R(R-\Delta)}, \tag{23}$$

$$f(\pm\pi) = \frac{1}{(4\pi c)^2}\frac{n_C(\pm\pi)}{4\pi^2 R(R+\Delta)}, \tag{24}$$

$$\psi(0) = -\frac{\Delta}{c}, \tag{25}$$

$$\psi(\pm\pi) = \frac{\Delta}{c}, \tag{26}$$

$$\psi''(0) = \frac{\Delta R}{c(R-\Delta)}, \tag{27}$$

$$\psi''(\pm\pi) = -\frac{\Delta R}{c(R+\Delta)}. \tag{28}$$

To obtain equations (25)–(28), one must also recall that $\sqrt{R^2 + \Delta^2 - \Delta R\cos\varphi} = r_{2S}$ is, physically, a positive distance: when $\varphi = 0, \pm\pi$, it follows that $\sqrt{R^2 + \Delta^2 - 2\Delta R} = R - \Delta$.

Substituting expressions (23)–(28) into equation (22), we find after some algebra that

$$I_C(\omega) \approx \frac{1}{(4\pi c)^2}\frac{1}{2\pi}\sqrt{\frac{c}{2\pi\Delta R^3}}\left[n_C(\pi)\frac{\mathrm{e}^{\mathrm{i}\left(\frac{\omega\Delta}{c}-\frac{\pi}{4}\right)}}{\sqrt{(R+\Delta)\omega}} + n_C(0)\frac{\mathrm{e}^{-\mathrm{i}\left(\frac{\omega\Delta}{c}-\frac{\pi}{4}\right)}}{\sqrt{(R-\Delta)\omega}}\right], \tag{29}$$

where the sign of $\pi/4$ in the argument of the exponential function was selected based on the sign of ψ'' as explained in section A1. Comparing equation (29) with (E17), it is apparent that both terms at the right-hand side of (29) are proportional to the high-frequency/far-field form of the Green's function $G_{2D}(\Delta, \omega)$ (and, interestingly, not G_{3D}).

Equation (21) and the subsequent expressions for $I_C(\omega)$ are only valid for large and positive ω so that $I_C(\omega)$ remains undefined for $\omega < 0$. We know, however, that a sum of cross correlations of real-valued functions of time should be real valued in the time domain, requiring that $I_C(\omega) = I_C^*(-\omega)$, and

$$F^{-1}[I_C(\omega)] = \frac{1}{\sqrt{2\pi}}\int_{-\infty}^{+\infty} \mathrm{d}\omega\, I_C(\omega)\mathrm{e}^{\mathrm{i}\omega t} = \frac{1}{\sqrt{2\pi}}\left(\int_0^{+\infty} \mathrm{d}\omega\, I_C(\omega)\mathrm{e}^{\mathrm{i}\omega t} + \int_0^{+\infty} \mathrm{d}\omega\, I_C^*(\omega)\mathrm{e}^{-\mathrm{i}\omega t}\right) \tag{30}$$

After substituting (29) into (30), the integration over ω can be conducted analytically, making use of the identity

$$\int_0^{\infty} \mathrm{d}x\, \frac{\mathrm{e}^{\mathrm{i}ax}}{\sqrt{x}} = \begin{cases} \frac{1}{\sqrt{a}}\sqrt{\frac{\pi}{2}}(1+\mathrm{i}) & \text{if } a > 0, \\ \frac{1}{\sqrt{-a}}\sqrt{\frac{\pi}{2}}(1-\mathrm{i}) & \text{if } a < 0, \end{cases} \tag{31}$$

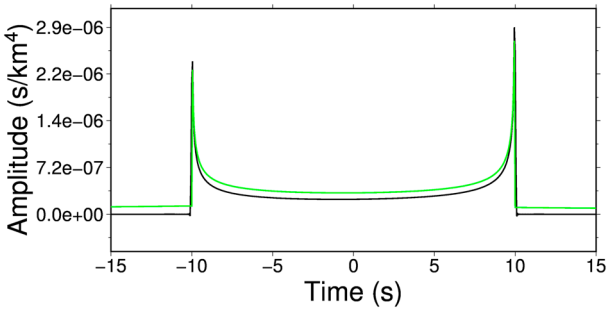

Figure 5. Source-averaged cross correlations associated with a circular, planar distribution of sources surrounding the two receivers, obtained (green line) implementing equation (32), compared with (black) the real part of that resulting from the numerical approach of section 4.1 (shown already in Figure 2). The source/station setup is the same as for Figure 2.

and integrating separately for the three cases $t < -\frac{\Delta}{c}$, $-\frac{\Delta}{c} < t < \frac{\Delta}{c}$ and $t > \frac{\Delta}{c}$. After a considerable amount of algebra we find

$$I_C(t) = \frac{1}{(4\pi c)^2}\frac{1}{2\pi}\sqrt{\frac{c}{\pi\Delta R^3}} \times \begin{cases} \frac{n_C(0)}{\sqrt{R-\Delta}}\frac{1}{\sqrt{\frac{\Delta}{c}-t}} & \text{if } t < -\frac{\Delta}{c}, \\ \frac{n_C(\pi)}{\sqrt{R+\Delta}}\frac{1}{\sqrt{\frac{\Delta}{c}+t}} + \frac{n_C(0)}{\sqrt{R-\Delta}}\frac{1}{\sqrt{\frac{\Delta}{c}-t}} & \text{if } -\frac{\Delta}{c} < t < \frac{\Delta}{c}, \\ \frac{n_C(\pi)}{\sqrt{R+\Delta}}\frac{1}{\sqrt{\frac{\Delta}{c}+t}} & \text{if } t > \frac{\Delta}{c}, \end{cases} \tag{32}$$

which, as required, has zero imaginary part. We infer from equation (32) that in the current setup, there is no explicit relationship between the source-averaged cross correlation $I_C(t)$ and the Green's functions G_{2D} or G_{3D} (Appendix E). Figure 5 shows that $I_C(t)$ as obtained from equation (32) is consistent with the numerical result of Figure 2. The discussion of section 4.1 remains valid. A slight discrepancy between the "analytical" and "numerical" results in Figure 5 is explained by the stationary-phase approximation being strictly valid only at high frequency ($\omega \longrightarrow \infty$).

5.2. Sources Over a Spherical Surface

The integral in equation (9) can be solved analytically with the help of equation (A12). Equation (9) is indeed a particular case of (A3), with $x = \theta, y = \varphi, \lambda = \omega, f(\theta,\varphi) = n_S \sin\theta/[8\pi^2(r_{2S}(\theta,\varphi) - r_{1S}(\theta,\varphi))]$, and $\psi(\theta,\varphi) = \left[r_{2S}(\theta,\varphi) - r_{1S}(\theta,\varphi)\right]/c$. Again, the reference frame is centered on $R1$ so that $r_{1S}(\theta,\varphi) = R$ for all values of θ and φ. After some algebra, we find

$$r_{2S} = \left(R^2 + \Delta^2 - 2\Delta R\sin\theta\cos\varphi\right)^{\frac{1}{2}}, \tag{33}$$

and consequently

$$f(\theta,\varphi) = \frac{1}{(4\pi c)^2}\frac{n_S(\theta,\varphi)\,\sin\theta}{8\pi^2 R\,\left(R^2 + \Delta^2 - 2\Delta R\sin\theta\cos\varphi\right)^{\frac{1}{2}}}, \tag{34}$$

$$\psi(\varphi) = \frac{1}{c}(r_{2S} - r_{1S}) = \frac{1}{c}\left[\left(R^2 + \Delta^2 - 2\Delta R\sin\theta\cos\varphi\right)^{\frac{1}{2}} - R\right]. \tag{35}$$

Differentiating (35) with respect to θ and φ, we find

$$\psi_\theta = -\frac{\Delta R\cos\theta\cos\varphi}{c\,(R^2 + \Delta^2 - 2\Delta R\sin\theta\cos\varphi)^{\frac{1}{2}}}, \tag{36}$$

where the compact ψ_θ stands for $\frac{\partial\psi}{\partial\theta}$. Likewise,

$$\psi_\varphi = \frac{\Delta R\sin\theta\sin\varphi}{c\,(R^2 + \Delta^2 - 2\Delta R\sin\theta\cos\varphi)^{\frac{1}{2}}}. \tag{37}$$

If we continue differentiating,

$$\psi_{\theta\theta} = -\frac{\Delta R \cos^2\theta \cos^2\varphi}{c\,(R^2+\Delta^2-2\Delta R \sin\theta\cos\varphi)^{\frac{3}{2}}} + \frac{\Delta R \sin\theta\cos\varphi}{c\,(R^2+\Delta^2-2\Delta R \sin\theta\cos\varphi)^{\frac{1}{2}}}, \tag{38}$$

$$\psi_{\varphi\varphi} = -\frac{\Delta R \sin^2\theta \sin^2\varphi}{c\,(R^2+\Delta^2-2\Delta R \sin\theta\cos\varphi)^{\frac{3}{2}}} + \frac{\Delta R \sin\theta\cos\varphi}{c\,(R^2+\Delta^2-2\Delta R \sin\theta\cos\varphi)^{\frac{1}{2}}}, \tag{39}$$

$$\psi_{\theta\varphi} = \frac{\Delta R \sin\theta \sin\varphi \cos\theta\cos\varphi}{c\,(R^2+\Delta^2-2\Delta R \sin\theta\cos\varphi)^{\frac{3}{2}}} + \frac{\Delta R \cos\theta\sin\varphi}{c\,(R^2+\Delta^2-2\Delta R \sin\theta\cos\varphi)^{\frac{1}{2}}}. \tag{40}$$

Equations (36) and (37) allow us to identify the stationary points $(\theta, \varphi$ such that $\psi_\theta, \psi_\varphi = 0, 0)$ of the integrand at the right-hand side of (9): namely, $(\theta = 0, \varphi = \pm\pi/2)$, $(\pi, \pm\pi/2)$, $(\pi/2, 0)$, and $(\pi/2, \pi)$. It is sufficient to evaluate (A12) at these points, and sum the results, to find an analytical expression for the integral (9). We notice first of all that $f(\theta, \varphi) = 0$ if $\theta = 0, \pm\pi$: the corresponding stationary points give no contribution to the integral and will be neglected in the following. We are left with the stationary points at $\theta = \pi/2$ and $\varphi = 0,\pi$. Let us evaluate $f, \psi, \psi_{\theta\theta}, \psi_{\varphi\varphi}$, and $\psi_{\theta\varphi}$ at those points.

$$f\left(\frac{\pi}{2}, 0\right) = \frac{1}{(4\pi c)^2}\frac{n_S\left(\frac{\pi}{2}, 0\right)}{8\pi^2 R\,(R-\Delta)}, \tag{41}$$

$$f\left(\frac{\pi}{2}, \pi\right) = \frac{1}{(4\pi c)^2}\frac{n_S\left(\frac{\pi}{2}, \pi\right)}{8\pi^2 R\,(R+\Delta)}, \tag{42}$$

$$\psi\left(\frac{\pi}{2}, 0\right) = -\frac{\Delta}{c}, \tag{43}$$

$$\psi\left(\frac{\pi}{2}, \pi\right) = \frac{\Delta}{c}, \tag{44}$$

$$\psi_{\theta\theta}\left(\frac{\pi}{2}, 0\right) = \frac{\Delta R}{c(R-\Delta)}, \tag{45}$$

$$\psi_{\theta\theta}\left(\frac{\pi}{2}, \pi\right) = -\frac{\Delta R}{c(R+\Delta)}, \tag{46}$$

$$\psi_{\varphi\varphi}\left(\frac{\pi}{2}, 0\right) = \frac{\Delta R}{c(R-\Delta)}, \tag{47}$$

$$\psi_{\varphi\varphi}\left(\frac{\pi}{2}, \pi\right) = -\frac{\Delta R}{c(R+\Delta)}, \tag{48}$$

and it follows immediately from (40) that $\psi_{\theta\varphi} = 0$ at all stationary points.

The above expressions can be substituted into (A12) to find

$$I_S(\omega) \approx \frac{1}{(4\pi c)^2}\frac{\mathrm{i}\,c}{4\pi R^2 \Delta}\left[n_S\left(\frac{\pi}{2}, 0\right)\frac{\mathrm{e}^{-\mathrm{i}\frac{\omega\Delta}{c}}}{\omega} - n_S\left(\frac{\pi}{2}, \pi\right)\frac{\mathrm{e}^{\mathrm{i}\frac{\omega\Delta}{c}}}{\omega}\right], \tag{49}$$

which satisfies $I_S(-\omega) = -I_S^*(\omega)$. Notice that substituting equation (E22) into (49),

$$I_S(\omega) \approx \frac{\sqrt{2\pi}}{(4\pi R)^2}\frac{\mathrm{i}}{\omega}\left[n_S\left(\frac{\pi}{2}, 0\right) G_{3D}(\Delta, \omega) - n_S\left(\frac{\pi}{2}, \pi\right) G_{3D}^*(\Delta, \omega)\right], \tag{50}$$

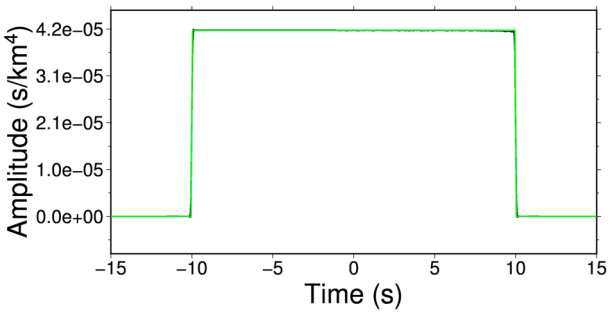

Figure 6. Stacked cross correlation resulting from a spherical distribution of sources surrounding the two receivers, predicted (green line) by the approximate analytical formula (53) and computed (black) numerically as described in section 4.2 and already illustrated in Figure 3 (only the real part is shown here). The source/station setup is the same as for Figure 3.

and if $n_S\left(\frac{\pi}{2},0\right)=n_S\left(\frac{\pi}{2},\pi\right)$, equation (50) can be further simplified to

$$I_S(\omega)\approx-\frac{\sqrt{2\pi}}{8\pi^2R^2}n_S\left(\frac{\pi}{2},0\right)\frac{1}{\omega}\Im\left[G_{3D}(\Delta,\omega)\right]. \tag{51}$$

We next inverse Fourier transform equation (49) to the time domain. In our convention,

$$\mathscr{F}^{-1}\left(\frac{1}{\omega}\right)=\mathrm{i}\sqrt{\frac{\pi}{2}}\mathrm{sgn}(t) \tag{52}$$

(Dirichlet integral), where the sign function sgn is +1 or −1 for positive and negative values of the argument, respectively. In the time domain, I_S is then

$$I_S(t)\approx\frac{1}{(4\pi c)^2}\frac{c}{4\sqrt{2\pi}\,R^2\,\Delta}\left[n_S\left(\frac{\pi}{2},\pi\right)\mathrm{sgn}\left(t+\frac{\Delta}{c}\right)-n_S\left(\frac{\pi}{2},0\right)\mathrm{sgn}\left(t-\frac{\Delta}{c}\right)\right], \tag{53}$$

illustrated in Figure 6. This result is consistent with equation (15) of *Roux et al.* [2005] and equation (27) of *Nakahara* [2006], who treated the same physical problem in different ways, and with Figure 1a of *Harmon et al.* [2008]. By comparison with equation (E21), it is apparent that the terms at the right-hand side of equation (53) are time integrals of the time domain Green's function $G_{3D}(\Delta,t)$. Equations (49) and (53) mean that the Green's function G_{3D} corresponding to propagation from receiver $R1$ to $R2$ and vice versa can be found by (i) recording at both receivers the signal emitted by a dense distribution of sources covering all azimuths in three dimensions; (ii) cross correlating, for each source, the signal recorded at R_1 with that recorded at R_2; and (iii) integrating the cross correlation over the source location **r**.

Our equation (49) coincides with equation (11) of *Snieder* [2004], except that here the difference between the right-hand side terms is taken, while in *Snieder* [2004] they are summed. Inverse Fourier transforming the formula of *Snieder* [2004] would lead to a nonphysical cross correlation, nonzero at times where cross correlation is necessarily zero at all φ. We infer that equations (11) and (12) in *Snieder* [2004] are wrong. However, this error did not affect the subsequent, Rayleigh wave derivation of *Snieder* [2004].

5.3. Membrane (or Rayleigh) Waves From 2-D Distribution of Point Sources

5.3.1. Source-Averaged Cross Correlation

We treat the integral in equation (10) with the stationary-phase method as illustrated in previous sections. The phase term $\psi(\varphi)$ in (10) is the additive inverse of that in (8), and the two integrands share the same stationary points $\varphi=0$ and $\varphi=\pm\pi$. At those points,

$$f(0)=\frac{n_M(0)}{32\pi^3c^3\omega\sqrt{R(R-\Delta)}}, \tag{54}$$

$$f(\pm\pi)=\frac{n_M(\pi)}{32\pi^3c^3\omega\sqrt{R(R+\Delta)}}, \tag{55}$$

$$\psi(0)=\frac{\Delta}{c}, \tag{56}$$

$$\psi(\pm\pi)=-\frac{\Delta}{c}, \tag{57}$$

$$\psi''(0)=-\frac{\Delta R}{c(R-\Delta)}, \tag{58}$$

$$\psi''(\pm\pi) = \frac{\Delta R}{c(R+\Delta)}. \tag{59}$$

Substituting into equation (A2) (which is multiplied by 2 for each stationary point) and summing over our set of two stationary points,

$$I_{MW}(\omega) \approx \frac{1}{16\pi^3 c^3 R}\sqrt{\frac{\pi c}{2\Delta}}\,\omega^{-\frac{3}{2}}\left[n_M(0)\mathrm{e}^{\mathrm{i}\left(\frac{\omega\Delta}{c}-\frac{\pi}{4}\right)} + n_M(\pi)\mathrm{e}^{-\mathrm{i}\left(\frac{\omega\Delta}{c}-\frac{\pi}{4}\right)}\right], \tag{60}$$

coherently with equations (23) and (24) of *Snieder* [2004], which, however, involve summation over normal modes. Comparing equation (60) with (E17), we can also write

$$I_{MW}(\omega) \approx \frac{\mathrm{i}}{4\pi^2\omega c R}\sqrt{\frac{\pi}{2}}\left[n_M(\pi)G_{2D}(\Delta,\omega) - n_M(0)G^*_{2D}(\Delta,\omega)\right], \tag{61}$$

valid in the asymptotic (high-frequency/far-field) approximation.

Equations (60) and (61) are valid in the stationary-phase approximation, i.e., for large and positive ω only. We know, however, that $I_{MW}(t)$ must be real: as in section 5.1, I_{MW} at $\omega < 0$ is thus defined by $I_{MW}(\omega) = I^*_{MW}(-\omega)$, and equation (30) remains valid after replacing I_C with I_{MW}, i.e.,

$$\mathscr{F}^{-1}[I_{MW}(\omega)] = \frac{1}{\sqrt{2\pi}}\left(\int_0^{+\infty}\mathrm{d}\omega\, I_{MW}(\omega)\mathrm{e}^{\mathrm{i}\omega t} + \int_0^{+\infty}\mathrm{d}\omega\, I^*_{MW}(\omega)\mathrm{e}^{-\mathrm{i}\omega t}\right). \tag{62}$$

After substituting the expression (60) for I_{MW} into (62), it becomes apparent that finding a time domain expression for I_{MW} requires the solution of a nonconvergent integral, namely, $\int_0^\infty \mathrm{d}x\, x^{-\frac{3}{2}}\cos(x)$.

5.3.2. Derivative of the Source-Averaged Cross Correlation

One can still use the present theoretical formulation to interpret 2-D data in the time domain, by simply taking the time derivative of both the observed source-averaged cross correlation and its analytical expression $I_{MW}(\omega)$. Based on the properties of Fourier transforms, the latter is achieved by multiplying $I_{MW}(\omega)$ by $\mathrm{i}\omega$,

$$I'_{MW}(\omega) \approx \frac{\mathrm{i}}{16\pi^3 c^3 R}\sqrt{\frac{\pi c}{2\Delta}}\left[n_M(0)\frac{\mathrm{e}^{\mathrm{i}\left(\frac{\omega\Delta}{c}-\frac{\pi}{4}\right)}}{\sqrt{\omega}} + n_M(\pi)\frac{\mathrm{e}^{-\mathrm{i}\left(\frac{\omega\Delta}{c}-\frac{\pi}{4}\right)}}{\sqrt{\omega}}\right]. \tag{63}$$

We infer from equation (63) that for acoustic waves in 2-D, and within the stationary-phase approximation, the derivative of the source-averaged cross correlation is proportional to the sum of causal and anticausal Green's functions $G_{2D}(\omega)$ given by equation (E17) [*Snieder*, 2004].

Like (60), equation (63) is only valid for large positive ω, but the fact that $I'_{MW}(t)$ is real can be used to define $I'_{MW}(\omega)$ at $\omega < 0$ via equation (30). The inverse Fourier transform of the resulting expression for $I'_{MW}(\omega)$ involves a convergent integral (equation (31)) and can be found analytically. The procedure is similar to that of section 5.1, equations (30)–(32). The result is quite different, as can be expected since the imaginary unit multiplies the right-hand side of equation (63). Namely,

$$I'_{MW}(t) \approx \frac{1}{16\pi^3 c^3 R}\sqrt{\frac{\pi c}{\Delta}} \times \begin{cases} \frac{n_M(0)}{\sqrt{-t-\frac{\Delta}{c}}} & \text{if } t < -\frac{\Delta}{c}, \\ 0 & \text{if } -\frac{\Delta}{c} < t < \frac{\Delta}{c}, \\ -\frac{n_M(\pi)}{\sqrt{t-\frac{\Delta}{c}}} & \text{if } t > \frac{\Delta}{c}. \end{cases} \tag{64}$$

Figure 7 shows that equation (64) is validated by the numerical results of section 4.3. No explicit mathematical relationship between I'_{MW} and G_{2D} can be inferred from equation (64), although Figure 7 shows that the behavior of the two functions is qualitatively similar.

5.3.3. Symmetric Source Distribution

Inverse Fourier transformation turns out to be easier when $n_M(\pi) = n_M(0)$: setting them both to 1 for simplicity, equation (61) collapses to

$$\begin{aligned} I_{MW}(\omega) &\approx \frac{\mathrm{i}}{4\pi^2\omega c R}\sqrt{\frac{\pi}{2}}\left[G_{2D}(\Delta,\omega) - G^*_{2D}(\Delta,\omega)\right] \\ &\approx -\frac{1}{2\pi^2\omega c R}\sqrt{\frac{\pi}{2}}\,\Im\left[G_{2D}(\Delta,\omega)\right], \end{aligned} \tag{65}$$

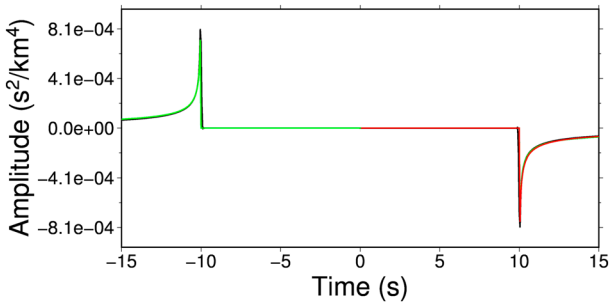

Figure 7. Time derivative $I'_{MW}(t)$ of the stacked cross correlation associated with a circular distribution of sources surrounding the two receivers on a membrane, predicted (green line) by the approximate analytical formula (64) and computed (black line) numerically as described in section 4.3 (Figure 4). Only the real parts are shown here since we have verified that imaginary parts are null as required by physics. For comparison, the Green's function $-G_{2D}$ from equation (E15) with $x = \Delta$ is also shown (red line); it is normalized so that its amplitude coincides with that of the numerical stack. The phase velocity and source/station setup are the same as for Figure 4.

and

$$I_{MW}(t) \approx -\frac{1}{2\pi^2 cR}\sqrt{\frac{\pi}{2}}\mathscr{F}^{-1}\left\{\frac{\Im\left[G_{2D}(\Delta,\omega)\right]}{\omega}\right\}. \tag{66}$$

Let us denote G^o_{2D} the odd function $G^o_{2D}(t) = \frac{1}{2}G_{2D}(t) - \frac{1}{2}G_{2D}(-t)$. We know from Appendix B, equation (B9), that $\Im\left[G_{2D}(\Delta,\omega)\right] = -\mathrm{i}G^o_{2D}(\Delta,\omega)$ so that

$$I_{MW}(t) \approx -\frac{1}{2\pi^2 cR}\sqrt{\frac{\pi}{2}}\mathscr{F}^{-1}\left[\frac{-\mathrm{i}G^o_{2D}(\Delta,\omega)}{\omega}\right]. \tag{67}$$

It also follows from Appendix B, equation (B4), that

$$\mathscr{F}^{-1}\left[\frac{-\mathrm{i}G^o_{2D}(\Delta,\omega)}{\omega}\right] = \int_{-\infty}^{t} G^o_{2D}(\tau)\mathrm{d}\tau, \tag{68}$$

and by definition of G^o_{2D},

$$I_{MW}(t) \approx -\frac{1}{4\pi^2 cR}\sqrt{\frac{\pi}{2}}\left\{\int_{-\infty}^{t}\left[G_{2D}(\tau) - G_{2D}(-\tau)\right]\mathrm{d}\tau\right\}. \tag{69}$$

Differentiating with respect to time,

$$I'_{MW}(t) \approx \frac{1}{4\pi^2 cR}\sqrt{\frac{\pi}{2}}\left[G_{2D}(-t) - G_{2D}(t)\right], \tag{70}$$

consistent with Figure 7. The apparent discrepancy between equations (64) and (70) is explained by the fact that the derivation of (70) involved identifying G_{2D} with its asymptotic approximation (E17), which was not the case for the derivation of equation (64).

5.4. Plane Waves

5.4.1. Exact Integration

An elegant way of reducing equation (15) to a simple and useful identity is to compare it with the integral form of the zeroth-order Bessel function of the first kind,

$$J_0(z) = \frac{1}{\pi}\int_0^{\pi}\mathrm{d}\varphi\ \cos(z\cos\varphi) \tag{71}$$

[*Abramowitz and Stegun*, 1964, equation (9.1.18)]. Substituting (71) into (15),

$$I_{PW}(\omega) = \sqrt{\frac{\pi}{2}}\,q(\omega)J_0\left(\frac{\omega\Delta}{c}\right), \tag{72}$$

an exact equality that does not require the stationary-phase approximation. Importantly, equation (72) was originally obtained in the early study of *Aki* [1957], providing the basis for much of the later work in ambient noise seismology. Comparing (72) with (E16), we infer that the source-averaged cross correlation $I_{PW}(\omega)$ is proportional to the imaginary part of the membrane wave Green's function $G_{2D}\left(\frac{\omega r}{c}\right)$ if $r = \Delta$.

5.4.2. Approximate Integration

In analogy with previous sections, the integral in equation (15) can also be solved by means of the stationary-phase approximation. Let us rewrite it

$$I_{PW}(\omega) = \frac{q(\omega)}{\sqrt{2\pi}}\,\Re\left[\int_0^\pi \mathrm{d}\varphi\, \mathrm{e}^{\mathrm{i}\omega\frac{\Delta\cos\varphi}{c}}\right]. \tag{73}$$

The integral at the right-hand side of equation (73) coincides with that in (A1) after replacing $a = 0$, $b = \pi$, $x = \varphi$, $\lambda = \omega$, and $\psi(\varphi) = \frac{\Delta\cos\varphi}{c}$. Taking the φ derivative of ψ,

$$\psi_\varphi(\varphi) = -\frac{\Delta}{c}\sin\varphi, \tag{74}$$

and we see immediately that there are two stationary points within the integration domain, at the integration limits $\varphi = 0,\pi$. Differentiating again, we find

$$\psi_{\varphi\varphi}(\varphi) = -\frac{\Delta}{c}\cos\varphi. \tag{75}$$

At the stationary point $\varphi = 0$ we have $\psi(0) = \frac{\Delta}{c}$ and $\psi_{\varphi\varphi}(0) = -\frac{\Delta}{c}$. At $\varphi = \pi$, $\psi(0) = -\frac{\Delta}{c}$ and $\psi_{\varphi\varphi}(0) = \frac{\Delta}{c}$. For each stationary point, we substitute the corresponding values into equation (A2), choosing, as usual, the sign of $\pi/4$ in the argument of the exponential based on that of $\psi_{\varphi\varphi}$. We next sum the contributions of both stationary points, finding

$$\int_0^\pi \mathrm{d}\varphi\, \mathrm{e}^{\mathrm{i}\omega\frac{\Delta\cos\varphi}{c}} \approx \sqrt{\frac{2\pi\, c}{\omega\Delta}}\,\cos\left(\frac{\omega\Delta}{c} - \frac{\pi}{4}\right). \tag{76}$$

Substituting, in turn, (76) into (73),

$$I_{PW}(\omega) \approx q(\omega)\sqrt{\frac{c}{\omega\Delta}}\,\cos\left(\frac{\omega\Delta}{c} - \frac{\pi}{4}\right) \approx \sqrt{\frac{\pi}{2}}\,q(\omega)\,J_0\left(\frac{\omega\Delta}{c}\right), \tag{77}$$

where we have used the asymptotic approximation of J_0 [*Abramowitz and Stegun*, 1964, equation (9.2.1)], valid in the high-frequency (and/or far-field) limit, i.e., in the range of validity of the stationary-phase approximation. Equation (77) shows that the stationary-phase approximation leads to an estimate of source-averaged cross correlation $I_{PW}(\omega)$ consistent, at large ω, with the result (72).

The relationship (72) between observed stacked cross correlations and the Bessel's function J_0 has been applied, e.g., by *Ekström et al.* [2009] and *Ekström* [2014] to analyze ambient noise surface wave data in the frequency domain and measure their velocity. The inverse Fourier transform of (72) is obtained and discussed by *Nakahara* [2006], who also shows that the Hilbert transform of the stacked cross correlation coincides with the (causal minus anticausal) G_{2D} [*Nakahara*, 2006, equation (19)].

5.4.3. Monochromatic Plane Waves in the Time Domain

The treatments of *Sanchez-Sesma and Campillo* [2006], *Tsai* [2009], and *Boschi et al.* [2013] are slightly different from the plane wave formulation presented here, in that they work with monochromatic plane waves in the time domain. Following *Tsai* [2009], *Boschi et al.* [2013] make use of the properties of the Bessel and Struve functions to solve the integral in equation (13) and are eventually able to write the source-averaged cross correlation of plane waves of frequency ω_0 traveling along all azimuths as

$$I_{TD}(\omega_0, t) = q(\omega_0)\sqrt{\frac{c}{8\pi\omega_0\Delta}}\left\{\cos\left[\omega_0\left(t + \frac{\Delta}{c}\right) - \frac{\pi}{4}\right] + \cos\left[\omega_0\left(t - \frac{\Delta}{c}\right) + \frac{\pi}{4}\right]\right\} \tag{78}$$

[*Boschi et al.*, 2013, equations (35) and (41)], valid in the far-field (large Δ) and/or high-frequency (large ω_0) approximations.

To verify that our equation (77) is consistent with (78), let us take the Fourier transform of the latter. From the equality $\mathcal{F}\left\{\cos[\omega_0(t+k)]\right\} = \sqrt{\frac{\pi}{2}}\left[\delta(\omega+\omega_0)+\delta(\omega-\omega_0)\right]\mathrm{e}^{-\mathrm{i}\omega k}$ it follows that

$$I_{TD}(\omega_0,\omega) = \frac{q(\omega_0)}{2}\sqrt{\frac{c}{\omega_0\Delta}}\left[\delta(\omega+\omega_0)+\delta(\omega-\omega_0)\right]\cos\left[\omega\left(\frac{\pi}{4\omega_0}-\frac{\Delta}{c}\right)\right]. \tag{79}$$

Like (14), equation (79) is valid for any ω_0. Implicitly repeating the monochromatic wave, time domain analysis at all ω_0's,

$$I_{TD}(\omega) = q(\omega)\sqrt{\frac{c}{\omega\Delta}}\cos\left(\frac{\omega\Delta}{c}-\frac{\pi}{4}\right), \tag{80}$$

which coincides, as expected, with our expression (77) for $I_{PW}(\omega)$.

6. Other Derivations

6.1. Time Domain Approach

We loosely follow the treatment of *Roux et al.* [2005, section II], with acoustic sources uniformly distributed throughout an unbounded, infinite 3-D medium. This setup is similar to section 5.2 here. Although in section 5.2 sources are all lying on the surface of a sphere (azimuthally uniform distribution), we show in the following that the formula we find for the source-averaged cross correlation is proportional to that derived by *Roux et al.* [2005].

In free 3-D space, the time domain cross correlation between impulsive signals emitted at S and recorded at $R1$ and $R2$ (i.e., the time domain version of equation (6)) reads

$$\begin{aligned}\frac{1}{T}\int_{-\frac{T}{2}}^{+\frac{T}{2}}\mathrm{d}\tau\, G_{3D}(r_{1S},\tau)G_{3D}(r_{2S},t+\tau) &= \frac{1}{(4\pi c)^2}\frac{1}{T}\int_{-\frac{T}{2}}^{+\frac{T}{2}}\mathrm{d}\tau\,\frac{\delta\left(\tau-\frac{r_{1S}}{c}\right)\delta\left(\tau+t-\frac{r_{2S}}{c}\right)}{r_{1S}\,r_{2S}}\\ &= \frac{1}{(4\pi c)^2}\frac{1}{T}\frac{\delta\left(t+\frac{r_{1S}}{c}-\frac{r_{2S}}{c}\right)}{r_{1S}\,r_{2S}},\end{aligned} \tag{81}$$

where we have used expression (E21) for G_{3D}, and we have limited cross correlation to a finite time interval $(-T/2, T/2)$, whose length T is related, in practice, to interstation distance and wave speed.

As discussed in section 3, if cross terms are neglected (Appendix D), the cross correlation of a diffuse wavefield recorded at $R1$ and $R2$ is estimated by summing expression (81) over many uniformly distributed sources S. For sources densely distributed throughout the entire 3-D space $\mathbb{R}^3$,

$$I_{3D}(t) = \frac{1}{(4\pi c)^2}\frac{1}{T}\int_{\mathbb{R}^3}\mathrm{d}^3\mathbf{r}\,\frac{\delta\left(t+\frac{r_{1S}}{c}-\frac{r_{2S}}{c}\right)}{r_{1S}\,r_{2S}}, \tag{82}$$

where $\mathbf{r}$ is the source location, and, said $\mathbf{r}_1$ and $\mathbf{r}_2$, respectively, the locations of $R1$ and $R2$, $r_{1S}=|\mathbf{r}-\mathbf{r}_1|$, $r_{2S}=|\mathbf{r}-\mathbf{r}_2|$. Equation (82) is equivalent to equation (9) of *Roux et al.* [2005].

As noted by *Roux et al.* [2005], equation (82) shows that a wiggle in the cross correlation I_{3D} at time t is necessarily associated to one or more sources whose location $\mathbf{r}$ satisfies $ct = |\mathbf{r}-\mathbf{r}_2| - |\mathbf{r}-\mathbf{r}_1|$. In two dimensions, the latter is the equation of a hyperbola with foci at $R1$ at $R2$; in three dimensions, it is the equation of the single-sheet hyperboloid obtained by rotation of said hyperbola around the vertical axis. It follows that the integral in (82) can be reduced to a surface integral over the hyperboloid. After this simplification, *Roux et al.* [2005] are able to solve the integral in (82) analytically: they find $I_{3D}(t)$ to be a boxcar function between $t = \pm\Delta/c$, equivalent to equation (49) in section 5.2 here.

6.2. Reciprocity Theorem Approach

All descriptions of seismic and acoustic interferometry that we discussed so far rest on equation (1) and on the Green's function formulae of Appendix E, which are strictly valid only for g, infinite media. More general formulations have been developed by *Wapenaar* [2004], *Weaver and Lobkis* [2004], *van Manen et al.* [2005],

Wapenaar and Fokkema [2006], *Snieder* [2007], and others, based on the reciprocity or Betti's theorem [e.g., *Aki and Richards*, 2002, section 2.3.2].

6.2.1. Acoustic Waves

The propagation of acoustic waves in a nonhomogeneous, lossless stagnant gas of density ρ and compressibility κ is described by equation (6.2.7) of *Morse and Ingard* [1986], plus the forcing term q corresponding to mass injection. In the frequency domain,

$$\nabla p + \mathrm{i}\omega\rho\mathbf{v} = \mathbf{0}, \tag{83}$$

$$\nabla \cdot \mathbf{v} + \mathrm{i}\omega\kappa p - q = 0. \tag{84}$$

In the more general case of a sound-absorbing medium, κ is complex and its imaginary part is proportional to the rate of energy loss (attenuation) [*Kinsler et al.*, 1999, chap. 8]. Equations (83) and (84) are equivalent to equations (2) and (3) of *Wapenaar and Fokkema* [2006] or equations (1) and (2) of *Snieder* [2007] where a different Fourier transform convention applies. Equation (83) implies $\mathbf{v} = \frac{1}{\mathrm{i}\omega\rho}\nabla p$, and this expression for $\mathbf{v}$ can be substituted into (84), to obtain

$$\nabla \cdot \left(\frac{1}{\rho}\nabla p\right) + \omega^2\kappa p = -\mathrm{i}\omega q. \tag{85}$$

For homogeneous or smooth media, where the spatial derivatives of ρ and κ are zero or approximately zero, (85) further simplifies to the Fourier transform of equation (1),

$$\frac{1}{\rho}\nabla^2 p + \omega^2\kappa p = -\mathrm{i}\omega q. \tag{86}$$

Following *Wapenaar and Fokkema* [2006], let us call $\mathscr{G}$ the solution of (86) when $q(\mathbf{x}, t) = \delta(\mathbf{x})\delta(t)$:

$$\frac{1}{\rho}\nabla^2\mathscr{G} + \omega^2\kappa\mathscr{G} = -\mathrm{i}\omega\delta(\mathbf{x}). \tag{87}$$

$\mathscr{G}$ can be interpreted as the Green's function associated with equation (84) plus the condition (83).

The relationship between $\mathscr{G}$ and G_{3D} as defined in Appendix E can be determined if one considers that equation (87) is the usual scalar wave equation (whose Green's function is G_{3D}) with forcing term $-\mathrm{i}\omega\delta(\mathbf{x})$; based on equation (E34), the time domain solution to (87) is then the convolution of G_{3D} with the inverse Fourier transform of the forcing term $-\mathrm{i}\omega\delta(\mathbf{x})$; in the frequency domain the convolution reduces to the product of the functions in question, and

$$\mathscr{G} = -\mathrm{i}\omega G_{3D}. \tag{88}$$

Wapenaar and Fokkema [2006] also introduce a "modified Green's function" (see their equation (32)) which coincides with our G_{3D} except for the sign.

Let us next consider a volume V bounded by a surface ∂V. (∂V is just an arbitrary closed surface within a medium and generally does not represent a physical boundary.) Let $q_A(\mathbf{r}, \omega)$, $p_A(\mathbf{r}, \omega)$, and $\mathbf{v}_A(\mathbf{r}, \omega)$ denote a possible combination of forcing, pressure, and velocity, respectively, coexisting at $\mathbf{r}$ in V and ∂V. A different forcing q_B would give rise, through equations (83) and (84), to a different "state" B, defined by $p_B(\mathbf{r}, \omega)$ and $\mathbf{v}_B(\mathbf{r}, \omega)$.

A useful relationship between the states A and B, known as "reciprocity theorem," is obtained by combining equations (83) and (84) as follows:

$$\int_V \mathrm{d}^3\mathbf{r}\left[(83)_A \cdot \mathbf{v}_B^* + (83)_B^* \cdot \mathbf{v}_A + (84)_A\, p_B^* + (84)_B^*\, p_A\right] = 0 \tag{89}$$

[e.g., *Wapenaar and Fokkema*, 2006; *Snieder*, 2007], where $(83)_A$ is short for the expression one obtains after substituting $p = p_A(\mathbf{r}, \omega)$ and $\mathbf{v} = \mathbf{v}_A(\mathbf{r}, \omega)$ into the left-hand side of equation (83), etc. Namely,

$$(83)_A \cdot \mathbf{v}_B^* = \nabla p_A \cdot \mathbf{v}_B^* + \mathrm{i}\omega\rho\mathbf{v}_A \cdot \mathbf{v}_B^* \tag{90}$$

$$(83)^*_B \cdot \mathbf{v}_A = \nabla p^*_B \cdot \mathbf{v}_A - \mathrm{i}\omega\rho \mathbf{v}^*_B \cdot \mathbf{v}_A \tag{91}$$

$$(84)_A\, p^*_B = \nabla \cdot \mathbf{v}_A\, p^*_B + \mathrm{i}\omega\kappa p_A p^*_B - q_A p^*_B \tag{92}$$

$$(84)^*_B\, p_A = \nabla \cdot \mathbf{v}^*_B\, p_A - \mathrm{i}\omega\kappa^* p^*_B p_A - q^*_B p_A. \tag{93}$$

Since $(83)_A = (83)_B = (84)_A = (84)_B = 0$ by virtue of equation (83) and (84), it follows that the expression at the left-hand side of (89) equals 0 as anticipated. After substituting (90)–(93) into (89),

$$\begin{aligned} &\int_V \mathrm{d}^3\mathbf{r}\left(\nabla p_A \cdot \mathbf{v}^*_B + \nabla \cdot \mathbf{v}^*_B p_A\right) + \int_V \mathrm{d}^3\mathbf{r}\left(\nabla p^*_B \cdot \mathbf{v}_A + \nabla \cdot \mathbf{v}_A p^*_B\right) \\ &- \int_V \mathrm{d}^3\mathbf{r}\, \mathrm{i}\omega(\kappa^* - \kappa) p_A p^*_B - \int_V \mathrm{d}^3\mathbf{r}\left(q_A p^*_B + q^*_B p_A\right) = 0. \end{aligned} \tag{94}$$

It is convenient to apply the divergence theorem [e.g., *Hildebrand*, 1976] to the first two integrals at the left-hand side of equation (94), which then simplifies to

$$\int_{\partial V} \mathrm{d}^2\mathbf{r}\,(p_A \mathbf{v}^*_B + p^*_B \mathbf{v}_A) \cdot \hat{\mathbf{n}} + 2\mathrm{i}\omega \int_V \mathrm{d}^3\mathbf{r}\, \Im(\kappa) p_A p^*_B - \int_V \mathrm{d}^3\mathbf{r}\,(q^*_B p_A + q_A p^*_B) = 0, \tag{95}$$

where $\hat{\mathbf{n}}$ is the unit vector normal to ∂V and $\Im(\kappa)$ denotes the imaginary part of κ. Equation (95) is equivalent to the "reciprocity theorem of the convolution type," equation (5) of *Wapenaar and Fokkema* [2006] or equation (4) of *Snieder* [2007].

An equation relating the cross correlation of ambient signal to Green's functions can be found from (95) by considering the case $q_{A,B}(\mathbf{r}) = \delta(\mathbf{r} - \mathbf{r}_{A,B})$, with $\mathbf{r}_{A,B}$ arbitrary locations in V. It follows that $p_{A,B} = \mathscr{G}(\mathbf{r}, \mathbf{r}_{A,B})$. Substituting these expressions for p and q into (95) and using (83) to eliminate the velocity,

$$\begin{aligned} &\mathscr{G}(\mathbf{r}_B, \mathbf{r}_A) + \mathscr{G}^*(\mathbf{r}_A, \mathbf{r}_B) = \\ &= \frac{1}{\mathrm{i}\omega} \int_{\partial V} \mathrm{d}^2\mathbf{r}\, \frac{1}{\rho} \left[\mathscr{G}^*(\mathbf{r}, \mathbf{r}_B) \nabla \mathscr{G}(\mathbf{r}, \mathbf{r}_A) - \mathscr{G}(\mathbf{r}, \mathbf{r}_A) \nabla \mathscr{G}^*(\mathbf{r}, \mathbf{r}_B)\right] \cdot \hat{\mathbf{n}} \\ &+ 2\mathrm{i}\omega \int_V \mathrm{d}^3\mathbf{r}\, \Im(\kappa) \mathscr{G}(\mathbf{r}, \mathbf{r}_A) \mathscr{G}^*(\mathbf{r}, \mathbf{r}_B) \end{aligned} \tag{96}$$

[e.g., *Wapenaar and Fokkema*, 2006; *Snieder*, 2007; *Campillo and Roux*, 2014].

Notice that the treatment that leads from equation (89) to (96) remains valid for heterogeneous κ and ρ; equation (96) holds for a heterogeneous, attenuating medium that could be bounded or unbounded. It is thus more general than similar equations (32), (53), (63), and (72), which are only strictly valid if the propagation medium is homogeneous.

Provided that the medium be smooth or homogeneous at and near ∂V, $\mathscr{G}$ still coincides with $-\mathrm{i}\omega G_{3D}$ on ∂V, with G_{3D} the homogeneous medium Green's function. $\nabla\mathscr{G} = -\mathrm{i}\omega\nabla G_{3D}$ can then be computed through equation (E22), which implies

$$\nabla G_{3D}(\mathbf{r}, \omega) = \frac{\mathbf{r}}{r}\left[\frac{2}{r} G_{3D}(\mathbf{r}, \omega) - \frac{\mathrm{i}\omega}{c} G_{3D}(\mathbf{r}, \omega)\right]. \tag{97}$$

If we make the further assumption that all sources are far from ∂V (r is always large), it follows that $\frac{2}{r} G_{3D}$ can be neglected in equation (97), while $\frac{\mathbf{r}}{r} \cdot \hat{\mathbf{n}} \approx 1$ so that

$$\nabla G_{3D}(\mathbf{r}, \omega) \cdot \hat{\mathbf{n}} \approx -\frac{\mathrm{i}\omega}{c} G_{3D}(\mathbf{r}, \omega), \tag{98}$$

and

$$\nabla \mathscr{G}(\mathbf{r}, \omega) \cdot \hat{\mathbf{n}} \approx -\frac{\mathrm{i}\omega}{c} \mathscr{G}(\mathbf{r}, \omega) \tag{99}$$

[e.g., *Wapenaar and Fokkema*, 2006; *Snieder*, 2007; *Campillo and Roux*, 2014]. The surface integral in equation (96) is accordingly simplified,

$$\begin{aligned} &\mathcal{G}(\mathbf{r}_B,\mathbf{r}_A)+\mathcal{G}^*(\mathbf{r}_A,\mathbf{r}_B)= \\ &\approx -\frac{2}{\rho c}\int_{\partial V} \mathrm{d}^2\mathbf{r}\,\left[\mathcal{G}^*(\mathbf{r},\mathbf{r}_B)\mathcal{G}(\mathbf{r},\mathbf{r}_A)\right] \\ &+2\mathrm{i}\omega\int_V \mathrm{d}^3\mathbf{r}\,\Im(\kappa)\mathcal{G}(\mathbf{r},\mathbf{r}_A)\mathcal{G}^*(\mathbf{r},\mathbf{r}_B). \end{aligned} \tag{100}$$

Our treatment in section (5.2) was limited to nonattenuating media, where $\Im(\kappa) = 0$. In this case equation (100) reduces to

$$\mathcal{G}(\mathbf{r}_B,\mathbf{r}_A)+\mathcal{G}^*(\mathbf{r}_A,\mathbf{r}_B)\approx -\frac{2}{\rho c}\int_{\partial V}\mathrm{d}^2\mathbf{r}\,\left[\mathcal{G}^*(\mathbf{r},\mathbf{r}_B)\mathcal{G}(\mathbf{r},\mathbf{r}_A)\right]. \tag{101}$$

Applying equation (88), i.e., replacing $\mathcal{G} = -\mathrm{i}\omega G_{3D}$,

$$\frac{\mathrm{i}\rho c}{2\omega}\left[G^*_{3D}(\mathbf{r}_A,\mathbf{r}_B)-G_{3D}(\mathbf{r}_B,\mathbf{r}_A)\right]=-\int_{\partial V}\mathrm{d}^2\mathbf{r}\,\left[G^*_{3D}(\mathbf{r},\mathbf{r}_B)G_{3D}(\mathbf{r},\mathbf{r}_A)\right], \tag{102}$$

and by virtue of the reciprocity $G_{3D}(\mathbf{r}_B,\mathbf{r}_A)=G_{3D}(\mathbf{r}_A,\mathbf{r}_B)$, etc.,

$$\frac{\rho c}{\omega}\Im[G_{3D}(\mathbf{r}_A,\mathbf{r}_B)]=-\int_{\partial V}\mathrm{d}^2\mathbf{r}\,\left[G^*_{3D}(\mathbf{r},\mathbf{r}_B)G_{3D}(\mathbf{r},\mathbf{r}_A)\right]. \tag{103}$$

The right-hand side of equation (103) is simply $I_S(\omega)$ as defined by equation (9); since n_S in equation (51) is arbitrary, equations (103) and (51) are equivalent. In a smooth, lossless medium illuminated from all azimuths, the stationary-phase and reciprocity theorem approaches lead to the same relationship between Green's function and cross correlation, establishing, in practice, that the Green's function between $\mathbf{r}_A$ and $\mathbf{r}_B$ can be reconstructed from observations as long as the medium is illuminated by a dense distribution of sources covering its boundary ∂V (section 5.2).

The more general, reciprocity theorem-based results (96) and/or (100) apply to attenuating media. $\Im(\kappa)\neq 0$ implies that the volume integrals at their right-hand sides cannot be neglected; reconstruction of an attenuating medium's Green's function from the data requires that the medium be illuminated by sources *within V* [e.g., *Campillo and Roux*, 2014].

6.2.2. Seismic Waves

In a series of articles, Kees Wapenaar and coworkers have applied the above ideas to the case of an elastic medium, where both compressional and shear deformation exist [e.g., *Wapenaar*, 2004; *Wapenaar and Fokkema*, 2006; *Wapenaar et al.*, 2006]. Their procedure, based on applying the reciprocity theorem to a pair of states both excited by impulsive point sources, is qualitatively similar to the acoustic wave formulation of *Snieder* [2007], illustrated here in section 6.2.1. The most complete description of the reciprocity theorem approach is that of *Wapenaar et al.* [2006], who allow for medium inhomogeneity and attenuation. *Wapenaar et al.* [2006] show that in analogy with equations (100)–(103) for the acoustic case, the Green's function can be reconstructed from noise cross correlation provided that the medium is illuminated by noise sources densely distributed throughout a volume V, where receivers are immersed. If the medium is lossless, sources within V are unnecessary, but illumination from sources distributed throughout the surface that bounds V is still needed.

6.3. Normal-Mode Approach

Lobkis and Weaver [2001] use a normal-mode approach to find an analytical expression for diffuse field cross correlation in a bounded medium. Following *Snieder et al.* [2010], we briefly repeat their treatment for the simpler case of a lossless bounded medium. Normal modes are defined as the real functions $p_n(\mathbf{r})$ such that $p_n(\mathbf{r})\cos(\omega_n t)$, $p_n(\mathbf{r})\sin(\omega_n t)$ (n=1,2,3,… , ∞), with eigenfrequencies ω_n, form a complete set of solutions to the homogenous version of the scalar wave equation (1). Any wavefield $p(\mathbf{r},t)$ propagating in the medium under consideration can be written as a linear combination of modes with coefficients a_n, b_n

$$p(\mathbf{r},t)=\sum_n\left[a_n p_n(\mathbf{r})\cos(\omega_n t)+b_n p_n(\mathbf{r})\sin(\omega_n t)\right], \tag{104}$$

where $\sum_n$ denotes summation over the integer values of n from 1 to infinity.

6.3.1. Green's Function as a Linear Combination of Modes

Let us define the Green's function G_M as the solution of the homogeneous version ($\frac{\partial F}{\partial t} = 0$) of equation (1), with initial conditions $p = 0$ and $\frac{\partial p}{\partial t} = \delta(\mathbf{r}-\mathbf{s})$ (point source at $\mathbf{s}$). $G_M(\mathbf{r}, t)$ can be written as a linear combination of modes,

$$G_M(\mathbf{r}, t) = \sum_k \left[\alpha_k \cos(\omega_k t) + \beta_k \sin(\omega_k t)\right] p_k(\mathbf{r}). \tag{105}$$

Substituting into (105) the initial condition on p, we find

$$\sum_k \alpha_k p_k(\mathbf{r}) = 0; \tag{106}$$

after differentiating (105) with respect to time, the initial condition on $\frac{\partial p}{\partial t}$ gives

$$\sum_k \omega_k \beta_k p_k(\mathbf{r}) = \delta(\mathbf{r} - \mathbf{s}). \tag{107}$$

We multiply both sides of equations (106) and (107) by the eigenfunction $p_n(\mathbf{r})$ and integrate over $\mathbf{r}$. From equation (107) we find

$$\sum_k \omega_k \beta_k \int_{\mathbb{R}^3} \mathrm{d}^3\mathbf{r}\, p_k(\mathbf{r}) p_n(\mathbf{r}) = \int_{\mathbb{R}^3} \mathrm{d}^3\mathbf{r}\, \delta(\mathbf{r} - \mathbf{s}) p_n(\mathbf{r}), \tag{108}$$

which, after taking advantage of the orthonormality of the modes (left-hand side) and applying the properties of the δ function (right-hand side), collapses to

$$\beta_n \omega_n = p_n(\mathbf{s}). \tag{109}$$

Equation (106) likewise reduces to $\alpha_k = 0$, and equation (105) becomes

$$G_M(\mathbf{r}, t) = \sum_n p_n(\mathbf{s}) p_n(\mathbf{r}) \frac{\sin(\omega_n t)}{\omega_n}, \tag{110}$$

valid for $t > 0$, consistent with equation (4) of *Lobkis and Weaver* [2001] and equation (1) of *Snieder et al.* [2010].

6.3.2. Ensemble-Averaged Cross Correlation as a Linear Combination of Modes

Let us write the ambient signals recorded at $R1$ and $R2$ as linear combinations of modes with random coefficients a_n and b_n. Their cross correlation then reads

$$\begin{aligned}\int_{-T/2}^{+T/2} \mathrm{d}\tau\, p^*(\mathbf{r}_1, \tau) p(\mathbf{r}_2, t+\tau) = \sum_{n,k} \Bigg\{ & a_k a_n p_k(\mathbf{r}_1) p_n(\mathbf{r}_2) \int_{-T/2}^{+T/2} \mathrm{d}\tau \cos(\omega_k \tau) \cos[\omega_n (t+\tau)] \\ & + a_k b_n p_k(\mathbf{r}_1) p_n(\mathbf{r}_2) \int_{-T/2}^{+T/2} \mathrm{d}\tau \cos(\omega_k \tau) \sin[\omega_n (t+\tau)] \\ & + b_k a_n p_k(\mathbf{r}_1) p_n(\mathbf{r}_2) \int_{-T/2}^{+T/2} \mathrm{d}\tau \sin(\omega_k \tau) \cos[\omega_n (t+\tau)] \\ & + b_k b_n p_k(\mathbf{r}_1) p_n(\mathbf{r}_2) \int_{-T/2}^{+T/2} \mathrm{d}\tau \sin(\omega_k \tau) \sin[\omega_n (t+\tau)] \Bigg\}.\end{aligned} \tag{111}$$

Lobkis and Weaver [2001] make the assumption that "modal amplitudes are uncorrelated random variables," which is equivalent to noise sources being spatially and temporally uncorrelated so that "cross terms" can be neglected (Appendix D). This means in practice that if one repeats the cross correlation (111) at many different times, the normal modes of the medium stay the same (medium properties do not change), but the coefficients a_n and b_n change in a random fashion at each realization. When the average of all realizations is taken, the products $a_k a_n$ and $b_k b_n$ both average to $\delta_{kn} M(\omega_n)$, with the function M indicating how strongly different

eigenfrequencies are excited on average, and $\delta_{kn} = 1$ if $k = n$, 0 otherwise; $a_k b_n$, on the other hand, averages to 0 for all values of k, n. Using $\langle \bullet \rangle$ to denote the averaging procedure, it follows from (111) that

$$\begin{aligned}\langle \int_{-T/2}^{+T/2} \mathrm{d}\tau\, p^*(\mathbf{r}_1,\tau)p(\mathbf{r}_2,t+\tau)\rangle &= \sum_{n,k}\Big\{\langle a_k a_n\rangle p_k(\mathbf{r}_1)p_n(\mathbf{r}_2)\int_{-T/2}^{+T/2}\mathrm{d}\tau\cos(\omega_k\tau)\cos[\omega_n(t+\tau)]\\ &+\langle a_k b_n\rangle p_k(\mathbf{r}_1)p_n(\mathbf{r}_2)\int_{-T/2}^{+T/2}\mathrm{d}\tau\cos(\omega_k\tau)\sin[\omega_n(t+\tau)]\\ &+\langle b_k a_n\rangle p_k(\mathbf{r}_1)p_n(\mathbf{r}_2)\int_{-T/2}^{+T/2}\mathrm{d}\tau\sin(\omega_k\tau)\cos[\omega_n(t+\tau)]\\ &+\langle b_k b_n\rangle p_k(\mathbf{r}_1)p_n(\mathbf{r}_2)\int_{-T/2}^{+T/2}\mathrm{d}\tau\sin(\omega_k\tau)\sin[\omega_n(t+\tau)]\Big\}\\ &=\sum_n M(\omega_n)p_n(\mathbf{r}_1)p_n(\mathbf{r}_2)\int_{-T/2}^{+T/2}\mathrm{d}\tau\cos(\omega_n t)\\ &=\sum_n M(\omega_n)p_n(\mathbf{r}_1)p_n(\mathbf{r}_2)T\cos(\omega_n t),\end{aligned} \tag{112}$$

where the trigonometric identity $\cos(\omega_n\tau)\cos[\omega_n(t+\tau)] + \sin(\omega_n\tau)\sin[\omega_n(t+\tau)] = \cos(\omega_n t)$ is used [*Snieder et al.*, 2010]. Equation (111) is equivalent to equations (9) or (10) of *Snieder et al.* [2010], except that we have chosen not to normalize the coefficients a_n and b_n by the corresponding eigenfrequency ω_n.

Provided that M is constant with respect to ω (all modes are equally excited), the time derivative of the right-hand side of equation (112) is proportional to the right-hand side of (110): in other words, the ensemble-averaged cross correlation of a diffuse field recorded at $\mathbf{r}_1$ and $\mathbf{r}_2$ is proportional to the time derivative of the Green's function G_M (equation (110) in section 6.3.1), for a source located at $\mathbf{r}_1$ and a receiver located at $\mathbf{r}_2$. This is equivalent to equations (50) and (103), valid for nonsteady state 3-D acoustic media.

6.4. Analogy Between Diffuse Field and Time-Reversal Mirror

Derode et al. [2003] explain the relationship between diffuse field cross correlation and Green's function via the concept of time-reversal mirror [e.g., *Fink*, 1999, 2006]. A time-reversal mirror can be thought of as an array of transducers that record sound, reverse it with respect to time, and emit the time-reversed acoustic signal; if the array is sufficiently large and dense, it will time reverse the entire propagating wavefield, focusing time-reversed waves back to the origin of the initial signal.

Following *Stehly* [2007], we next summarize the reasoning of *Derode et al.* [2003] in three simple steps. First of all (section 6.4.1), cross correlating two signals is equivalent to time reversing the first signal then convolving it with the second. We then show (section 6.4.2) that the convolution of two impulsive signals emitted from $\mathbf{r}$ and recorded at the locations $\mathbf{r}_1$ and $\mathbf{r}_2$ coincides with the signal recorded at $\mathbf{r}_2$ after being emitted by a source at $\mathbf{r}_1$ and then time reversed and reemitted by a transducer at $\mathbf{r}$. It follows (section 6.4.3) that if instead of a single transducer at $\mathbf{r}$ an entire array of transducers forming a time-reversal mirror are present, the mentioned convolution coincides with the Green's function: through the relationship between convolution and cross correlation, an equation connecting Green's function and cross correlation is thus determined.

6.4.1. Convolution, Cross Correlation, and Time Reversal

Let us first recall the definition of the convolution $f \otimes g$ of two real-valued functions $f(t)$, $g(t)$:

$$f \otimes g(t) = \int_{-\infty}^{+\infty} f(\tau)g(t-\tau)\mathrm{d}\tau. \tag{113}$$

It can be shown that the convolution operator is commutative,

$$f \otimes g = g \otimes f, \tag{114}$$

and associative,

$$(f \otimes g) \otimes h = f \otimes (g \otimes h). \tag{115}$$

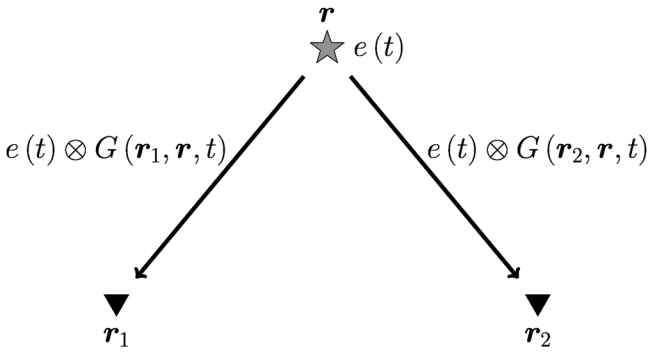

Figure 8. Setup of section 6.4.1, where a signal $e(t)$ emitted by a source at $\mathbf{r}$ (star) is recorded by receivers at $\mathbf{r}_1$ and $\mathbf{r}_2$ (triangles).

Convolution and cross correlation are closely related: if one denotes $f^-(t) \equiv f(-t)$ the function found by systematically changing the sign of the argument of f, that is to say, by time-reversing f, it follows that

$$\begin{aligned} f^- \otimes g(t) &= \int_{-\infty}^{+\infty} f(-\tau) g(t-\tau) \mathrm{d}\tau \\ &= -\int_{+\infty}^{-\infty} f(\tau) g(t+\tau) \mathrm{d}\tau \\ &= \int_{-\infty}^{+\infty} f(\tau) g(t+\tau) \mathrm{d}\tau, \end{aligned} \tag{116}$$

i.e., the convolution of f^- with g coincides with the cross correlation of f with g [e.g., *Smith*, 2011].

Now consider a source at the location $\mathbf{r}$ emitting the (real-valued) signal $e(t)$ and two receivers at the locations $\mathbf{r}_1$ and $\mathbf{r}_2$. By definition of Green's function G, the receiver at $\mathbf{r}_1$ records a signal $e \otimes G(\mathbf{r}_1, \mathbf{r})(t)$, while that at $\mathbf{r}_2$ records $e \otimes G(\mathbf{r}_2, \mathbf{r})(t)$ (Figure 8). Let us cross correlate the signal recorded at $\mathbf{r}_1$ with that recorded at $\mathbf{r}_2$ and denote C_{12} the cross correlation. Making use of equation (116) and of the fact that convolution is commutative and associative,

$$C_{12} = \left[e^- \otimes G^-(\mathbf{r}_1, \mathbf{r})(t)\right] \otimes \left[e \otimes G(\mathbf{r}_2, \mathbf{r})(t)\right] = \left[G^-(\mathbf{r}_1, \mathbf{r}) \otimes G(\mathbf{r}_2, \mathbf{r})(t)\right] \otimes \left[e^- \otimes e(t)\right]. \tag{117}$$

6.4.2. Propagation From One Source to a Transducer and From the Transducer to a Receiver

Let us now place at the location $\mathbf{r}_1$ a sound source that emits an impulsive signal, and at $\mathbf{r}$ a transducer that records sound, time reverses it, and emits it back (Figure 9). A receiver is still placed at $\mathbf{r}_2$. The signal recorded at $\mathbf{r}$ coincides with the Green's function $G(\mathbf{r}, \mathbf{r}_1, t)$. The signal $p(\mathbf{r}_2, t)$ recorded at $\mathbf{r}_2$ at a time t is the convolution of the signal emitted by $\mathbf{r}$, that is, the time-reversed Green's function $G(\mathbf{r}, \mathbf{r}_1, -t)$, with the Green's function $G(\mathbf{r}_2, \mathbf{r}, t)$,

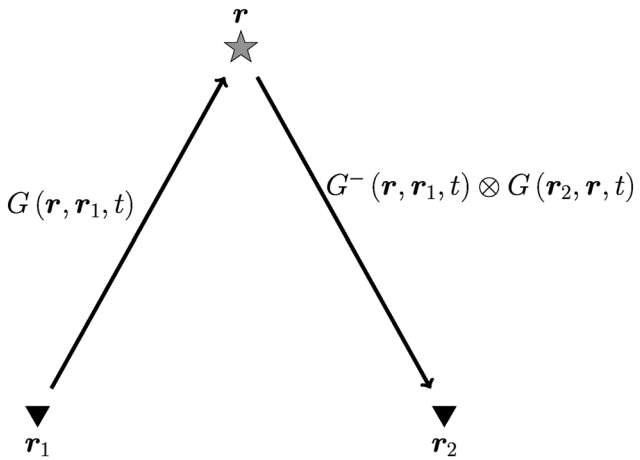

Figure 9. Setup of section 6.4.2, where an impulse emitted by a source at $\mathbf{r}_1$ (triangle) is recorded by a transducer at $\mathbf{r}$ (star), which then time reverses it and emits it back. A receiver at $\mathbf{r}_2$ (triangle) would then record the convolution of the time-reversed initial impulse with the Green's function corresponding to the locations $\mathbf{r}$ and $\mathbf{r}_2$.

$$p(\mathbf{r}_2, t) = G^-(\mathbf{r}, \mathbf{r}_1) \otimes G(\mathbf{r}_2, \mathbf{r})(t). \tag{118}$$

(This is valid in the assumption that the emitted wavelet is short enough and/or $\mathbf{r}$ is far enough from both $\mathbf{r}_1$ and $\mathbf{r}_2$ for the time-reversed wave packet $p(\mathbf{r}_2, t)$ to be easily isolated from the "direct" arrival at $\mathbf{r}_2$.) By the reciprocity of G, $G^-(\mathbf{r}, \mathbf{r}_1, t) = G^-(\mathbf{r}_1, \mathbf{r}, t)$. We can thus substitute equation (118) into (117), and

$$C_{12} = p(\mathbf{r}_2, t) \otimes \left[e^- \otimes e(t)\right], \tag{119}$$

i.e., the cross correlation of the recordings, made at $\mathbf{r}_1$ and $\mathbf{r}_2$, of the signal emitted by a source at $\mathbf{r}$ coincides with the recording made at $\mathbf{r}_2$ of the same signal, emitted at $\mathbf{r}_1$ and recorded and time reversed at $\mathbf{r}$. For impulsive signals $e(t) = \delta(t)$, equation (119) collapses to

$$C_{12} = p(\mathbf{r}_2, t). \tag{120}$$

6.4.3. Multiple Sources and Time-Reversal Mirror

We next consider a dense, uniform distribution of transducers surrounding the locations $\mathbf{r}_1$ and $\mathbf{r}_2$. Such a set of transducers forms a time-reversal mirror [e.g., *Fink*, 1999, 2006]. Equations (117) and (118) remain valid, after replacing $G(\mathbf{r}_1, \mathbf{r}, t)$, $G(\mathbf{r}_2, \mathbf{r}, t)$ with the sum of Green's functions associated with all locations $\mathbf{r}$ where transducers are now placed; at the limit of a continuous source distribution,

$$C_{12} = \int_\Omega \mathrm{d}\mathbf{r} \left[G^-(\mathbf{r}_1, \mathbf{r}) \otimes G(\mathbf{r}_2, \mathbf{r})(t)\right] \otimes \left[e^- \otimes e(t)\right], \tag{121}$$

where Ω is the entire solid angle.

In this setup (Figure 10), an impulsive signal emitted at $\mathbf{r}_1$ is first recorded at $\mathbf{r}_2$ as $G(\mathbf{r}_2, \mathbf{r}_1)$; it then hits the transducer array, which, by definition of time-reversal mirror, sends the signal back in such a way that the same wavefield propagates backward in time: the receiver at $\mathbf{r}_2$ records the time-reversed Green's function $G(\mathbf{r}_2, \mathbf{r}_1, -t)$, and the back-propagated signal eventually focuses back on $\mathbf{r}_1$ in the form of an impulse at time $-t = 0$.

This means, in practice, that if the individual transducer at $\mathbf{r}$ (Figure 8) is replaced by a time-reversal mirror, then $p(\mathbf{r}_2, t)$ in equation (120) can be replaced by the Green's function $G(\mathbf{r}_2, \mathbf{r}_1, -t)$,

$$C_{12} = G(\mathbf{r}_2, \mathbf{r}_1, -t). \tag{122}$$

Now recall from section 6.4.1 that C_{12} is also the cross correlation of the recordings made at $\mathbf{r}_1$ and $\mathbf{r}_2$ of signal generated at $\mathbf{r}$; the individual source at $\mathbf{r}$ must now be replaced by a set of sources occupying the transducer locations so that cross correlations associated with individual sources are summed. *Derode et al.* [2003] correctly infer that if a signal is generated by a distribution of sources with the geometry of an effective time-reversal mirror (i.e., energy propagating along all azimuths and diffuse field), the Green's function between any two points $\mathbf{r}_1$ and $\mathbf{r}_2$ can be found by cross correlating the recordings of the said signal made at $\mathbf{r}_1$ and $\mathbf{r}_2$. This statement is, again, equivalent to equations (50) and (103).

7. Uneven Source Distributions and "Spurious Arrivals"

Our derivation so far is based on the hypothesis that the geographic distribution of noise sources be close to uniform with respect to source-receiver azimuth. The stationary-phase formulae of Appendix A only hold if f is a *smooth* function of x in equation (A1) and of both x and y in equation (A3); the source distributions n_C, n_M, and n_S must accordingly be smooth with respect to φ and/or θ for the treatment of section 5 to be valid. The integral in equation (103) likewise extends to the whole boundary of the volume V containing the receivers: if ∂V is not covered densely and uniformly by sources, noise cross correlation does not coincide with the right-hand side of equation (103), and G is not properly reconstructed.

Noise sources are generally not uniformly distributed in practical applications, and we know, e.g., from *Mulargia* [2012], that seismic ambient noise on Earth is not strictly diffuse. We illustrate the consequences of significant inhomogeneities in source distribution with a simple model. As in sections 4.3 and 5.3, receivers $R1$ and $R2$, lying 20 km from one another on a membrane of infinite extension, are surrounded by a circle of sources whose center is $R1$ and whose radius is 100 km (Figure 11). We numerically convolve a Ricker wavelet (central frequency of 1 Hz) with the Green's function G_{2D} for each of the sources in question. Using a wavelet rather than an impulse allows to better visualize the effects we are interested in. For each location of the source, we cross correlate the corresponding signals at $R1$ and $R2$ and plot the cross correlations in Figure 12a. The result of stacking the cross correlations, shown in Figure 12b, is consistent with the results of section 5.3, after modulating the Green's function with the Ricker wavelet (we shall speak of "Ricker response" instead of Green's function). We next average only the cross correlations associated with sources denoted in green

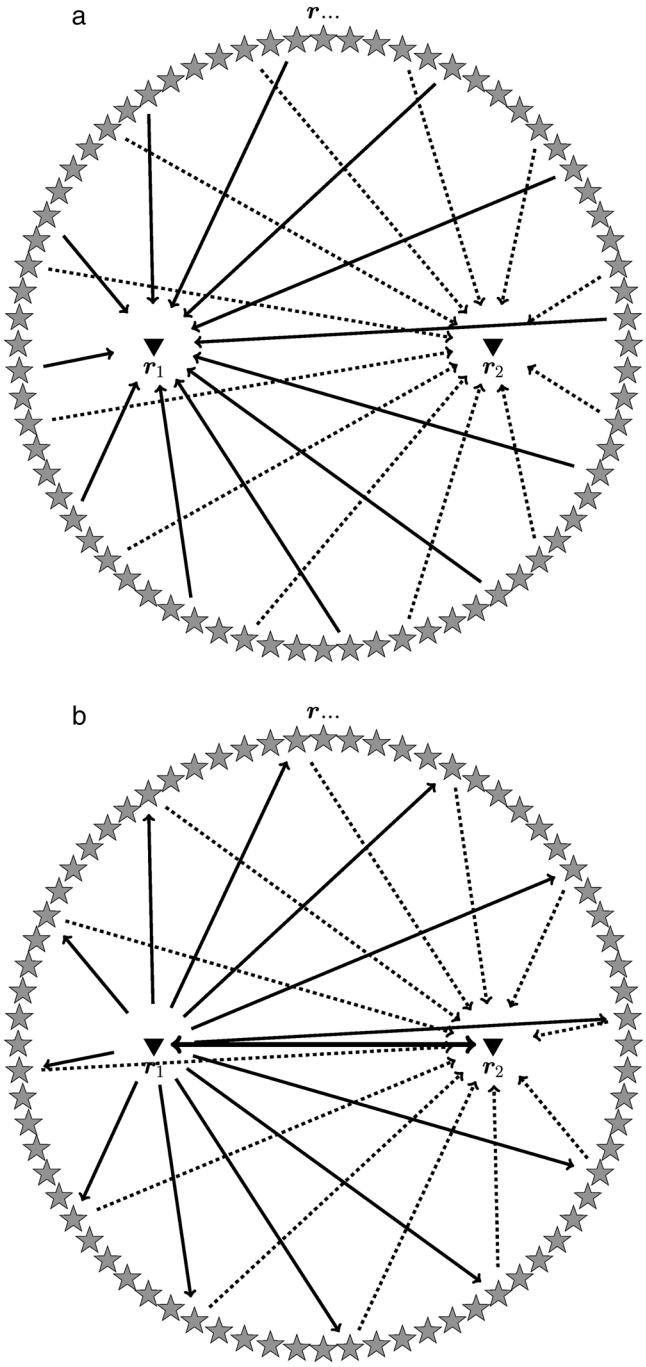

Figure 10. Setups of section 6.4.3. (a) Signals emitted by a circle of sources (stars) are recorded by a receiver pair at $\mathbf{r}_1$ and $\mathbf{r}_2$ (triangles); this is the same setup as in Figure 8 (section 6.4.1), but now there is more than one source. (b) An impulse emitted by a source at $\mathbf{r}_1$ is recorded by a set of transducers which time reverse it and emit it back. This is the same setup at in Figure 9 (section 6.4.2) but with more than one transducer. The transducers occupy the same locations (stars) as the sources in Figure 10a and thus form a time-reversal mirror (in two dimensions). *Derode et al.* [2003] and *Stehly et al.* [2006] use the properties of acoustic time reversal to prove that in a setup such as Figure 10a, the cross correlation between the signals recorded at $\mathbf{r}_1$ and $\mathbf{r}_2$ can be associated with the Green's function between the same two locations.

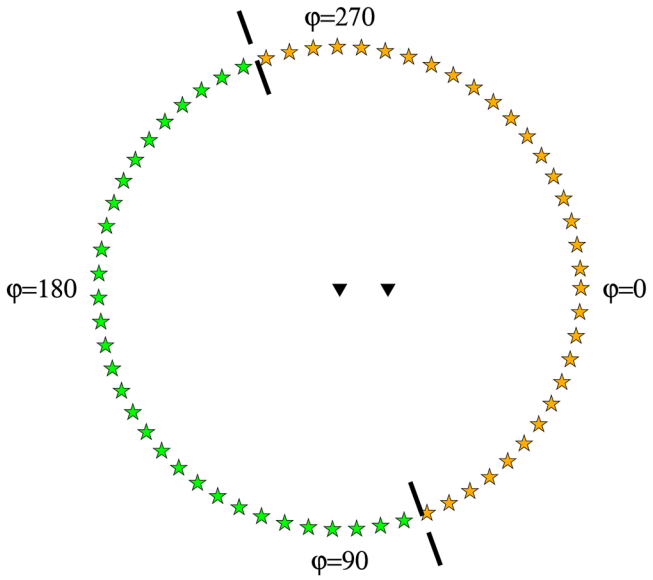

Figure 11. Distribution of sources (stars) and receivers (triangles) in the setup of section 7. Only 10% of the simulated sources are shown. In some of the simulations discussed in the following, the effects of uneven source distributions including only the sources denoted by green versus yellow stars are modeled.

in Figure 11 and, finally, only those associated with the "yellow" sources of Figure 11. Two inferences can be made from Figure 12c, where both averages are shown: (i) if only the yellow sources are "on," and energy only travels in the direction $R2 \longrightarrow R1$, only the anticausal Ricker's response between $R1$ and $R2$ emerges from averaging; likewise, only the causal part shows up if only sources to the left of $R1$ are active. (ii) While both causal and anticausal arrivals in Figure 12b approximately coincide with those of Figure 12c, the curves in Figure 12c contain two additional arrivals, corresponding to the two azimuths where both source distributions in Figure 11 abruptly end. These arrivals, usually referred to as spurious, have no relation to the Ricker response; they are artifacts caused by strong inhomogeneities in the source distribution. Spurious arrivals are likely to affect field data and can be identified in laboratory (physical acoustics) data.

8. Ambient Signal Cross Correlation in the Presence of a Scatterer: A Stationary-Phase Derivation

The stationary-phase derivations carried out above have established mathematical relationships between two-station ambient signal cross correlation and a medium's Green's function, in the simple case of *homogeneous*, unbounded media. The same approach can also usefully be applied to a homogeneous medium including a limited number of point scatterers. Following *Snieder et al.* [2008], we shall treat in some detail the case of a homogeneous, 3-D acoustic medium containing a single point scatterer: extension to more scatterers [*Fleury et al.*, 2010] is then straightforward, albeit cumbersome.

It is convenient to place the origin of the coordinate system at the location of the scatterer and to choose the x and z axes so that the plane they identify contains the locations $\mathbf{r}_1$, $\mathbf{r}_2$ of receivers $R1$ and $R2$. In this setup, the Green's function G^S_{3D} is the sum of G_{3D} from equation (E22) plus an additional, "scattered" term involving propagation from the source (located at a point $\mathbf{s}$) to the scatterer and from the scatterer to the receiver,

$$G^S_{3D}(\mathbf{r}_{1,2}, \mathbf{s}, \omega) = G_{3D}(r_{1,2S}, \omega) + G_{3D}(r_{1,2}, \omega) G_{3D}(s, \omega) h(\hat{\mathbf{r}}_{1,2}, \hat{\mathbf{s}}), \tag{123}$$

where $r_{1,2}$ and s denote the moduli of $\mathbf{r}_{1,2}$ and $\mathbf{s}$, respectively, and $\hat{\mathbf{r}}_{1,2}$, $\hat{\mathbf{s}}$ are unit vectors parallel to $\mathbf{r}_{1,2}$ and $\mathbf{s}$. The scattering function (or "matrix") $h(\hat{\mathbf{r}}_{1,2}, \hat{\mathbf{s}})$ accounts for the azimuth dependence of the amount of scattered energy [e.g., *Snieder*, 1986; *Groenenboom and Snieder*, 1995; *Marston*, 2001].

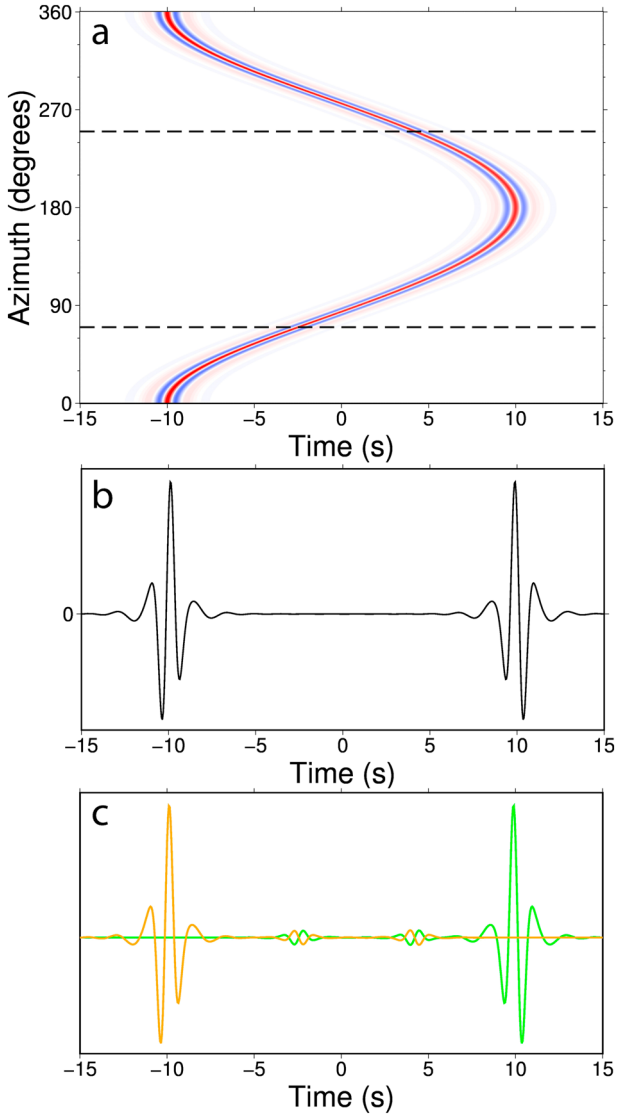

Figure 12. Cross correlations associated with a circular, planar distribution of sources surrounding the two receivers as sketched in Figure 11. Each source generates a Ricker wavelet (central frequency = 1 Hz); the wavelet is convolved with the Green's function (phase velocity $c = 2$ Km/s) to evaluate the signals observed at the two receivers, which are then cross correlated. (a) Single-source cross correlations for all source azimuths; the dashed lines mark the azimuths separating the two (yellow versus green) subsets of sources as defined in Figure 11. (b) Stacked cross correlation resulting from Figure 12a. (c) Stacked cross correlations that one would obtain if signal was generated only at the locations identified by green stars in Figure 11 (green line) versus the yellow stars (yellow line).

The frequency domain cross correlation of the signals recorded at $R1$ and $R2$ reads

$$\begin{aligned} G^{S}_{3D}(\mathbf{r}_1,\mathbf{s},\omega)G^{S*}_{3D}(\mathbf{r}_2,\mathbf{s},\omega) = {} & G_{3D}(r_{1S},\omega)G^{*}_{3D}(r_{2S},\omega) \\ & + G_{3D}(r_{1S},\omega)G^{*}_{3D}(r_2,\omega)G^{*}_{3D}(s,\omega)h^{*}(\hat{\mathbf{r}}_2,\hat{\mathbf{s}}) \\ & + G_{3D}(r_1,\omega)G_{3D}(s,\omega)G^{*}_{3D}(r_{2S},\omega)h(\hat{\mathbf{r}}_1,\hat{\mathbf{s}}) \\ & + G_{3D}(r_1,\omega)G_{3D}(s,\omega)G^{*}_{3D}(r_2,\omega)G^{*}_{3D}(s,\omega)h(\hat{\mathbf{r}}_1,\hat{\mathbf{s}})h^{*}(\hat{\mathbf{r}}_2,\hat{\mathbf{s}}). \end{aligned} \tag{124}$$

We next assume sources to be distributed over a spherical surface of radius $s = R$ surrounding the receivers, as in section 3, scenario (ii); for the sake of simplicity, we limit ourselves to uniform source density $n_S(\theta,\varphi) = 1$. Neglecting cross terms (Appendix D), the cumulative effect of such a source distribution is obtained by integrating equation (124) in $\mathbf{s}$ over the whole solid angle. The integral $I_S(\omega)$ of the first term at the right-hand side of (124) has been treated in detail in section 5.2, and its analytical form is given, e.g., by equation (50);

substituting $n_S(\theta,\varphi)=1$,

$$I_S(\omega)\approx\frac{\sqrt{2\pi}}{(4\pi R)^2}\frac{\mathrm{i}}{\omega}\left[G_{3D}(\Delta,\omega)-G^*_{3D}(\Delta,\omega)\right], \tag{125}$$

where Δ denotes, as usual, the distance between $R1$ and $R2$. Let us call $I_2(\omega)$, $I_3(\omega)$, and $I_4(\omega)$ the source averages of the remaining three terms at the right-hand side of (124). The first of these integrals,

$$\begin{aligned} I_2(\omega) &= \frac{1}{4\pi}\int_0^\pi \mathrm{d}\theta\sin\theta\int_{-\pi}^{\pi}\mathrm{d}\varphi\, G_{3D}(r_{1S}(\theta,\varphi),\omega)G^*_{3D}(r_2,\omega)G^*_{3D}(s(\theta,\varphi),\omega)h^*(\hat{\mathbf{r}}_2,\hat{\mathbf{s}}(\theta,\varphi)) \\ &= \frac{1}{(4\pi)^4}\frac{1}{\left(c\sqrt{2\pi}\right)^3}\int_0^\pi \mathrm{d}\theta\sin\theta\int_{-\pi}^{\pi}\mathrm{d}\varphi\,\frac{\mathrm{e}^{\mathrm{i}\frac{\omega}{c}(R+r_2-r_{1S}(\theta,\varphi))}}{R\,r_2\,r_{1S}(\theta,\varphi)}h^*(\hat{\mathbf{r}}_2,\hat{\mathbf{s}}(\theta,\varphi)), \end{aligned} \tag{126}$$

can be simplified by making the hypothesis that the source be very far from both receivers and from the scatterer [*Snieder et al.*, 2008], i.e., $R\gg r_{1,2}$, which implies that $r_{1,2S}$ can be replaced with R at the denominator of (126). At the exponent of the numerator care must be taken to evaluate the difference $R-r_{1S}$ which is of the same order as r_2; in the 3-D Cartesian reference frame

$$\mathbf{s}-\mathbf{r}_1=\left(R\sin\theta\cos\varphi-r_1\sin\theta_1, R\sin\theta\sin\varphi, R\cos\theta-r_1\cos\theta_1\right), \tag{127}$$

and consequently

$$r_{1S}=|\mathbf{s}-\mathbf{r}_1|=\left[R^2+r_1^2-2Rr_1(\sin\theta\cos\varphi\sin\theta_1+\cos\theta\cos\theta_1)\right]^{\frac{1}{2}}. \tag{128}$$

Equation (128) implies that

$$r_{1S}\approx R-r_1(\sin\theta\cos\varphi\sin\theta_1+\cos\theta\cos\theta_1) \tag{129}$$

to first order in r_1/R [*Snieder et al.*, 2008]. Substituting into equation (126),

$$I_2(\omega)=\frac{1}{(4\pi)^4}\frac{1}{\left(c\sqrt{2\pi}\right)^3R^2r_2}\mathrm{e}^{\mathrm{i}\frac{\omega}{c}r_2}\int_0^\pi\mathrm{d}\theta\sin\theta\int_{-\pi}^{\pi}\mathrm{d}\varphi\,\mathrm{e}^{\mathrm{i}\frac{\omega}{c}r_1(\sin\theta\cos\varphi\sin\theta_1+\cos\theta\cos\theta_1)}h^*(\hat{\mathbf{r}}_2,\hat{\mathbf{s}}(\theta,\varphi)). \tag{130}$$

The integral at the right-hand side of equation (130) coincides with that in equation (A3), after replacing $\lambda=\omega, x=\theta, y=\varphi$, $f(\theta,\varphi)=h^*(\hat{\mathbf{r}}_2,\hat{\mathbf{s}}(\theta,\varphi))\sin\theta$, and $\psi(\theta,\varphi)=r_1(\sin\theta\cos\varphi\sin\theta_1+\cos\theta\cos\theta_1)/c$; the stationary-phase formula (A2) can then be applied, provided that h be a *smooth* function of θ and φ.

In analogy with the procedure of section 5.2, we differentiate $\psi(\theta,\varphi)$ with respect to θ and φ to find the stationary points of (130),

$$\psi_\theta=\frac{r_1}{c}(\cos\theta\cos\varphi\sin\theta_1-\sin\theta\cos\theta_1), \tag{131}$$

$$\psi_\varphi=-\frac{r_1}{c}\sin\theta\sin\varphi\sin\theta_1. \tag{132}$$

Equation (132) establishes that stationary points can be found at either $\varphi=0$ or $\varphi=\pi$, i.e., on the plane where the scatterer and both receivers are. Substituting $\cos\phi=\pm1$ into equation (131), we further identify the two stationary points ($\theta=\theta_1$,$\varphi=0$) and ($\theta=\pi-\theta_1$,$\varphi=\pi$). If we continue differentiating,

$$\psi_{\theta\theta}=-\frac{r_1}{c}(\sin\theta\cos\varphi\sin\theta_1+\cos\theta\cos\theta_1), \tag{133}$$

$$\psi_{\varphi\varphi}=-\frac{r_1}{c}\sin\theta\cos\varphi\sin\theta_1, \tag{134}$$

$$\psi_{\theta\varphi}=\frac{r_1}{c}\sin\theta\sin\varphi\sin\theta_1. \tag{135}$$

At the stationary points,

$$\psi(\theta_1, 0) = \frac{r_1}{c}, \tag{136}$$

$$\psi(\pi - \theta_1, \pi) = -\frac{r_1}{c}, \tag{137}$$

$$\psi_{\theta\theta}(\theta_1, 0) = -\frac{r_1}{c}, \tag{138}$$

$$\psi_{\theta\theta}(\pi - \theta_1, \pi) = +\frac{r_1}{c}, \tag{139}$$

$$\psi_{\varphi\varphi}(\theta_1, 0) = -\frac{r_1}{c}\sin^2\theta_1, \tag{140}$$

$$\psi_{\varphi\varphi}(\pi - \theta_1, \pi) = \frac{r_1}{c}\sin^2\theta_1, \tag{141}$$

$$\psi_{\theta\varphi}(\theta_1, 0) = \psi_{\theta\varphi}(\pi - \theta_1, \pi) = 0. \tag{142}$$

After substituting (136)–(142) into the stationary-phase formula (A12),

$$I_2(\omega) \approx \frac{1}{(4\pi)^4}\frac{1}{\sqrt{2\pi}c^2R^2}\frac{e^{i\frac{\omega}{c}r_2}}{r_2}\frac{i}{\omega}\left[h^*(\hat{\mathbf{r}}_2, \hat{\mathbf{s}}(\pi - \theta_1, \pi))\frac{e^{-i\frac{\omega}{c}r_1}}{r_1} - h^*(\hat{\mathbf{r}}_2, \hat{\mathbf{s}}(\theta_1, 0))\frac{e^{i\frac{\omega}{c}r_1}}{r_1}\right]. \tag{143}$$

The integral in $I_3(\omega)$ is similar to that in $I_2(\omega)$, and the stationary-phase approximation leads to

$$I_3(\omega) \approx \frac{1}{(4\pi)^4}\frac{1}{\sqrt{2\pi}c^2R^2}\frac{e^{-i\frac{\omega}{c}r_1}}{r_1}\frac{i}{\omega}\left[h(\hat{\mathbf{r}}_1, \hat{\mathbf{s}}(\theta_2, 0))\frac{e^{-i\frac{\omega}{c}r_2}}{r_2} - h(\hat{\mathbf{r}}_1, \hat{\mathbf{s}}(\pi - \theta_2, \pi))\frac{e^{i\frac{\omega}{c}r_2}}{r_2}\right]. \tag{144}$$

The integral in $I_4(\omega)$,

$$I_4(\omega) = \frac{1}{(4\pi)^5}\frac{1}{(2\pi)^2c^4}\frac{e^{i\frac{\omega}{c}(r_2 - r_1)}}{R^2\, r_2\, r_1}\int_0^\pi d\theta \sin\theta \int_{-\pi}^{\pi} d\varphi\, h(\hat{\mathbf{r}}_1, \hat{\mathbf{s}}(\theta, \varphi))h^*(\hat{\mathbf{r}}_2, \hat{\mathbf{s}}(\theta, \varphi)), \tag{145}$$

is not a stationary-phase integral, in general.

Notice that by equation (E22) and since $\hat{\mathbf{s}}(\theta_1, 0) = \hat{\mathbf{r}}_2$, the term

$$\frac{e^{i\frac{\omega}{c}r_2}}{r_2}\frac{e^{i\frac{\omega}{c}r_1}}{r_1}h^*(\hat{\mathbf{r}}_1, \hat{\mathbf{s}}(\theta_1, 0)) = 2^5\pi^3c^2G^*_{3D}(r_2, \omega)G^*_{3D}(r_1, \omega)h^*(\hat{\mathbf{r}}_1, \hat{\mathbf{r}}_2), \tag{146}$$

appearing in (143), describes (the complex conjugate of) an impulse propagating from $R2$ to $R1$ via the scatterer. Likewise, in equation (144),

$$\frac{e^{-i\frac{\omega}{c}r_1}}{r_1}\frac{e^{-i\frac{\omega}{c}r_2}}{r_2}h(\hat{\mathbf{r}}_2, \hat{\mathbf{s}}(\theta_2, 0)) = 2^5\pi^3c^2G_{3D}(r_2, \omega)G_{3D}(r_1, \omega)h(\hat{\mathbf{r}}_2, \hat{\mathbf{r}}_1) \tag{147}$$

is an impulse propagating from $R1$ to $R2$ via the scatterer. The remaining terms in (143), (144), and (145) do not have an immediate physical explanation. The source-averaged cross correlation, coinciding with the integral of (124), takes the form

$$\begin{aligned} I_S(\omega)+I_2(\omega)+I_3(\omega)+I_4(\omega) \approx{}& \frac{\sqrt{2\pi}}{(4\pi R)^2}\frac{\mathrm{i}}{\omega}\left[G_{3D}(\Delta,\omega)-G^*_{3D}(\Delta,\omega)\right] \\ &-\frac{\sqrt{2\pi}}{(4\pi R)^2}\frac{\mathrm{i}}{\omega}G^*_{3D}(r_2,\omega)G^*_{3D}(r_1,\omega)h^*(\hat{\mathbf{r}}_1,\hat{\mathbf{r}}_2) \\ &+\frac{\sqrt{2\pi}}{(4\pi R)^2}\frac{\mathrm{i}}{\omega}G_{3D}(r_2,\omega)G_{3D}(r_1,\omega)h(\hat{\mathbf{r}}_2,\hat{\mathbf{r}}_1) \\ &+\frac{1}{(4\pi)^4}\frac{1}{\sqrt{2\pi}c^2}\frac{\mathrm{i}}{\omega}\frac{\mathrm{e}^{\mathrm{i}\frac{\omega}{c}(r_2-r_1)}}{R^2\,r_2\,r_1} \\ &\times\left\{\left[h^*(\hat{\mathbf{r}}_2,-\hat{\mathbf{r}}_1)-h(\hat{\mathbf{r}}_1,-\hat{\mathbf{r}}_2)\right]-\frac{1}{4\pi c^2}\frac{\omega}{(2\pi)^{\frac{3}{2}}}\int_0^\pi \mathrm{d}\theta\,\sin\theta\int_{-\pi}^{\pi}\mathrm{d}\varphi\,h(\hat{\mathbf{r}}_1,\hat{\mathbf{s}}(\theta,\varphi))h^*(\hat{\mathbf{r}}_2,\hat{\mathbf{s}}(\theta,\varphi))\right\} \end{aligned} \tag{148}$$

where we have used equation (49) with $n_S = 1$ and the identities $\hat{\mathbf{s}}(\pi-\theta_1,\pi) = -\mathbf{r}_1$ and $\hat{\mathbf{s}}(\pi-\theta_2,\pi) = -\mathbf{r}_2$.

Equation (148) was first derived, using a slightly different convention/notation, by *Snieder et al.* [2008], who observed that the term in $\{\dots\}$ is zero as a consequence of the generalized optical theorem. We are left with

$$\begin{aligned} I_S(\omega)+I_2(\omega)+I_3(\omega)+I_4(\omega) &\approx \frac{\sqrt{2\pi}}{(4\pi R)^2}\frac{\mathrm{i}}{\omega}\left[G^S_{3D}(\Delta,\omega)-G^{S*}_{3D}(\Delta,\omega)\right] \\ &\approx -\frac{\sqrt{2\pi}}{8(\pi R)^2}\frac{1}{\omega}\Im\left[G^S_{3D}(\Delta,\omega)\right], \end{aligned} \tag{149}$$

similar to equations (51) and (103). The procedure of section 5.3.3 could be applied to show that in the time domain, the source-averaged cross correlation (149) is proportional to the sum of $G^S_{3D}(t)$ (causal part) and $-G^S_{3D}(-t)$ (anticausal).

This result confirms that, as first pointed out by *Weaver and Lobkis* [2004], diffuse-field cross correlation in heterogeneous (rather than just homogeneous) media allows in principle to reconstruct the full Green's function of the medium, with all reflections and scatterings and propagation modes. This is implicit in the reciprocity theorem formulation of section 6.2 and has been verified experimentally and numerically by, e.g., *Larose et al.* [2006], *Mikesell et al.* [2012], and *Colombi et al.* [2014].

8.1. Spurious Arrivals and Their Cancelation

The result (149) might be surprising if one considers the scatterer as a ("secondary") source; no matter where the actual ("primary") source is, the scatterer is always at the same location relative to $R1$ and $R2$ so that the delay between the arrival of the scattered signal at $R1$ and its arrival at $R2$ is always the same. This would give rise to a peak in the stacked cross correlation that does not correspond with either of the two arrivals in G^S_{3D} as defined by equation (123).

This is illustrated in Figures 13 and 14. Following *Snieder et al.* [2008], we convolve a Ricker wavelet (central frequency of 1 Hz) with the Green's function associated with a uniformly dense, circular source distribution (Figure 13) plus a single scatterer. For simplicity and in analogy with *Snieder et al.* [2008], we work in two dimensions (membrane waves from point sources) and assume isotropic scattering. We implement the expression for h derived by *Groenenboom and Snieder* [1995] via the optical theorem [*Newton*, 2002]. For each location of the source, we cross correlate the corresponding signals at $R1$ and $R2$, which we choose to be equidistant from the scatterer, and plot the cross correlations in Figure 14a. As anticipated, whatever the source azimuth, a peak in the cross correlation appears at $t = 0$, corresponding to the scattered signal hitting simultaneously $R1$ and $R2$. This peak, or "arrival," at $t = 0$ clearly does not exist in G^S_{3D}, which would seem to contradict equation (149). However, when stacking all single-azimuth cross correlations, the $t = 0$ peak cancels out with the "knees" of some other cross correlation peaks (Figure 14b), and equation (149) is indeed confirmed. The four stationary points identified in section 8 appear as knees of the cross-correlation peaks in Figure 14a, corresponding in turn to the two causal and two anticausal peaks of the system's Ricker response (Figure 14b).

It is critical that source illumination be uniform, for the spurious term associated with the scatterer to disappear. To emphasize this point, we show in Figure 14c the stacks obtained by considering only half of the

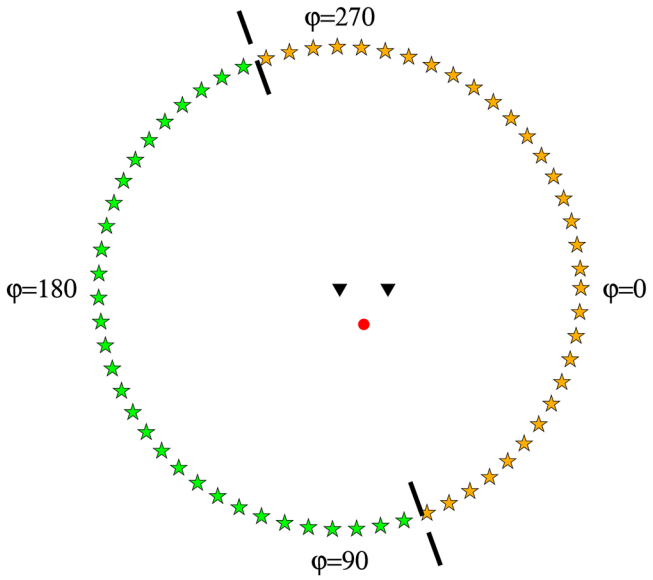

Figure 13. Distribution of sources (stars), receivers (triangles), and a point scatterer (red circle) in the setup of section 8.1. As in Figure 11, only 10% of the simulated sources are shown.

available sources [*Snieder et al.*, 2008], on either side of the receiver array. Depending on which side, only the causal or anticausal part of the Ricker response is reconstructed, as in Figure 12. Furthermore, three artifacts emerge; the one at $t = 0$ clearly results from the spurious wavelet in Figure 14a, which does not cancel out since the illumination is (strongly) nonuniform. The other two are simply the spurious arrivals of Figure 12, which result from the sharp inhomogeneities in source distribution, and would be found even in the absence of scatterers.

Scattering thus has a complex effect on Green's function reconstruction. Each scatterer further complicates the Green's function, introducing an additional, physical term to be reconstructed. It also hinders its retrieval, generating a spurious term which will only cancel out if the wavefield is sufficiently diffuse. On the other hand, scatterers themselves contribute to the wavefield's diffusivity and azimuthal uniformity of illumination. Recent and current work [e.g., *Fleury et al.*, 2010; *Mikesell et al.*, 2012; *Ravasi and Curtis*, 2013; *Colombi et al.*, 2014] aims at disentagling the specific role of scattered ambient signal in reconstructing the main peaks of the Green's function as well as its "coda."

9. Summary

In a diffuse ambient wavefield, i.e., a random wavefield where energy propagates with equal probability in all directions, cross correlating the signal recorded by a pair of receivers is a way to measure the impulse response (Green's function) between the receivers. In practice, long recordings of seismic ambient noise often include waves traveling along approximately all azimuths: the combination of their cross correlations approximates that of a diffuse field. The relationship between cross correlation and Green's function changes depending on some properties of the medium and of the wavefield:

(i) In a homogeneous, lossless, unbounded membrane where circular waves are generated by point sources, the cross correlation of diffuse noise is generally not explicitly related to the corresponding Green's function G_{2D} (section 5.3). If, however, the source distribution is symmetric along the receiver-receiver axis, equation (70) stipulates that G_{2D} is proportional to the time derivative of the cross correlation. The membrane setup is relevant to seismology, because it corresponds in practice to the propagation of Rayleigh waves (section 2.3) on Earth.

(ii) In homogeneous, lossless, unbounded 3-D acoustic media, the Green's function can be exactly reconstructed from diffuse noise generated at point sources that are smoothly distributed over a *sphere* surrounding the receivers. More precisely, the cross correlation coincides with the time derivative of the Green's function (section 5.2). This relationship holds for both causal and anticausal contributions to the

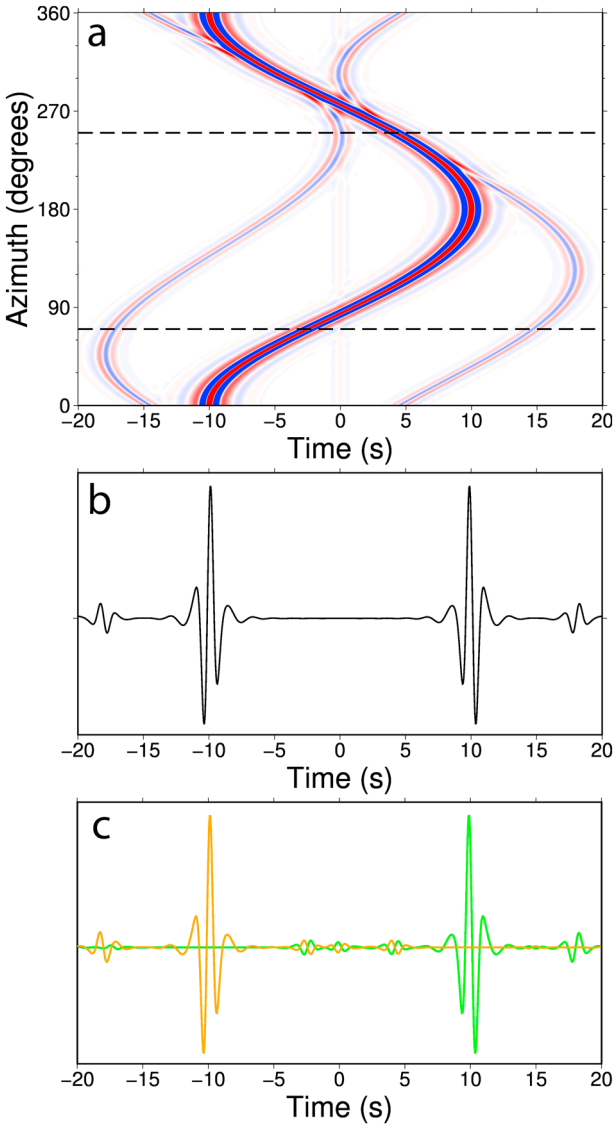

Figure 14. Cross correlations associated with a circular, planar distribution of sources surrounding the two receivers, and one isotropic point scatterer, as sketched in Figure 13. Each source generates a Ricker wavelet (central frequency = 1 Hz); the wavelet is convolved with the Green's function (phase velocity c = 2 Km/s), including the contribution of scattering, to evaluate the signals observed at the two receivers, which are then cross correlated. (a) Single-source cross correlations for all source azimuths; the color scale saturates at 20% of the maximum amplitude to emphasize the spurious arrivals; the dashed lines mark the azimuths where the yellow/"green" source distribution is discontinuous (Figure 13). (b) Source-averaged cross correlation resulting from Figure 14a. (c) Source-average cross correlations that one would obtain if signal was generated only at the locations identified by green stars in Figure 13 (green line) versus the yellow stars (yellow line).

Green's function/cross correlation and remains valid if the source distribution is asymmetric (provided that it be smooth).

(iii) The latter result does not hold if noise in free space is generated by point sources uniformly distributed along a *circle* surrounding the receivers (section 5.1). Still, even in this case, the time of maximum cross correlation clearly coincides with that of G_{2D}'s peak (Figure 5).

(iv) If noise is made up of *plane waves* propagating in all directions (section 5.4), the same formulation holds for 2-D and 3-D unbounded, lossless media. In this case, the source-averaged cross correlation is proportional, in the frequency domain, to the real part of the 2-D Green's function G_{2D}, which in turn is proportional to the Bessel function $J_0(\omega r/c)$, with r the interreceiver distance. Hence equation (72). The corresponding

time domain relationship was derived by *Nakahara* [2006], who showed that the Hilbert transform of diffuse field cross correlation coincides with the (causal minus anticausal) G_{2D}.

(v) In bounded, heterogeneous, attenuating media, a general relationship between source-averaged cross correlation and Green's function is found via the reciprocity theorem (section 6.2). Essentially, source-averaged cross correlation coincides with the sum of a volume (V) integral and an integral over the boundary ∂V of such volume. It follows that densely distributed noise sources *throughout a volume* are needed for the Green's function to be reconstructed via cross correlation; sources within V are unnecessary if the medium is lossless, provided that all *azimuths* are illuminated.

The results (i) and (iv) are relevant for most seismology applications seen so far, since, provided that attenuation can be neglected, they apply to surface waves in the "membrane" approximation [*Tanimoto*, 1990] (section 2.1). For example *Ekström et al.* [2009] have shown explicitly that the phase of the theoretical Green's function is in agreement with cross-correlated ambient noise data, thus validating the "lossless-medium" approximation for *phase/group-velocity*-based seismic imaging. Reconstructing the Green's function's *amplitude* remains problematic [e.g., *Weemstra et al.*, 2014].

Appendix A: The Stationary-Phase Approximation

A1. One-Dimensional Integrals

The stationary-phase approximation [e.g., *Bender and Orszag*, 1978] applies to integrals of the form

$$I(\lambda) = \int_a^b f(x) \mathrm{e}^{\mathrm{i}\lambda\psi(x)} \mathrm{d}x, \tag{A1}$$

where a and b are arbitrary constants and λ is large enough for $\mathrm{e}^{\mathrm{i}\lambda\psi(x)}$ to be a rapidly oscillating function of x, with respect to the smooth functions $f(x)$, $\psi(x)$. It is based on the finding [e.g., *Bender and Orszag*, 1978, section 6.5] that the leading contribution to $I(\lambda)$ comes from a small interval surrounding the "stationary points" of $\psi(x)$, i.e., the locations x such that $\psi'(x) = 0$ (where the "prime" denotes differentiation with respect to x). Elsewhere, the integrand oscillates quickly and its average contribution to the integral is negligible. *Bender and Orszag* [1978] demonstrate that for a single stationary point at a,

$$I(\lambda) \approx f(a) \mathrm{e}^{\mathrm{i}\left(\lambda\psi(a) \pm \frac{\pi}{4}\right)} \sqrt{\frac{\pi}{2\lambda|\psi''(a)|}}, \tag{A2}$$

valid for $\lambda \longrightarrow \infty$ and in the assumption that $\psi''(a) \neq 0$. The sign of $\pi/4$ at the exponent of e is positive if $\psi''(a) > 0$ and negative otherwise. Since any integral of the form (A1) can be written as a sum of integrals with one of the integration limits coinciding with a stationary point, equation (A2) is sufficient to solve all 1-D stationary-phase integrals like (A1), regardless of the number and location of stationary points [*Bender and Orszag*, 1978].

A2. Extension to 2-D Integrals

The result of section A1 can be used to find a general approximate formula for integrals of the form

$$I(\lambda) = \int_a^b \mathrm{d}x \int_c^d \mathrm{d}y f(x,y) \mathrm{e}^{\mathrm{i}\lambda\psi(x,y)}. \tag{A3}$$

If we, again, only consider the limit $\lambda \longrightarrow \infty$, the integrand in (A3) turns out to be very strongly oscillatory, and the only nonnegligible contribution to the integral comes from the vicinity of the stationary points (x_i, y_i), defined by

$$\left(\frac{\partial\psi}{\partial x}(x_i,y_i), \frac{\partial\psi}{\partial y}(x_i,y_i)\right) = (0,0) \tag{A4}$$

[e.g., *Wong*, 1986]. Equation (A3) can thus be approximated by

$$I(\lambda) \approx \sum_i f(x_i,y_i) \int_{x_i-\varepsilon}^{x_i+\varepsilon} \mathrm{d}x \int_{y_i-\delta}^{y_i+\delta} \mathrm{d}y \mathrm{e}^{\mathrm{i}\lambda\psi(x,y)}, \tag{A5}$$

where the sum is extended to all stationary points i, and ε and δ are small. $f(x,y)$ is approximated by $f(x_i,y_i)$ since f varies much more slowly than $\mathrm{e}^{\mathrm{i}\lambda\psi}$ when λ is large. We next conduct a Taylor series expansion of $\psi(x,y)$ around (x_i,y_i),

$$\psi(x,y) \approx \psi(x_i,y_i) + \frac{1}{2}\left[\psi_{xxi}(x-x_i)^2 + \psi_{yyi}(y-y_i)^2 + 2\psi_{xyi}(x-x_i)(y-y_i)\right], \tag{A6}$$

where ψ_{xxi} stands for $\frac{\partial^2\psi}{\partial x^2}(x_i, y_i)$, and so on. Substituting (A6) into (A5) and after the changes of variable $u_i = x - x_i$ and $v_i = y - y_i$, we find

$$I(\lambda) \approx \sum_i f(x_i, y_i) \mathrm{e}^{\mathrm{i}\lambda\psi(x_i,y_i)} \int_{-\epsilon}^{+\epsilon} \mathrm{d}u_i \int_{-\delta}^{+\delta} \mathrm{d}v_i \mathrm{e}^{\mathrm{i}\frac{\lambda}{2}\left(\psi_{xx}u_i^2 + \psi_{yy}v_i^2 + 2\psi_{xy}u_iv_i\right)}. \tag{A7}$$

The integral in (A7) can be solved analytically by first rewriting

$$\psi_{xxi}u_i^2 + \psi_{yyi}v_i^2 + 2\psi_{xyi}u_iv_i = \psi_{xxi}\left(u_i + \frac{\psi_{xyi}}{\psi_{xxi}}v_i\right)^2 + v_i^2\left(\psi_{yyi} - \frac{\psi_{xyi}^2}{\psi_{xxi}}\right), \tag{A8}$$

and substituting into (A7),

$$I(\lambda) \approx \sum_i f(x_i, y_i) \mathrm{e}^{\mathrm{i}\lambda\psi(x_i,y_i)} \int_{-\delta}^{+\delta} \mathrm{d}v_i \, \mathrm{e}^{\mathrm{i}\frac{\lambda}{2}v_i^2\left(\psi_{yyi} - \frac{\psi_{xyi}^2}{\psi_{xxi}}\right)} \int_{-\epsilon}^{+\epsilon} \mathrm{d}u_i \, \mathrm{e}^{\mathrm{i}\frac{\lambda}{2}\psi_{xxi}\left(u_i + \frac{\psi_{xyi}}{\psi_{xxi}}v_i\right)^2}. \tag{A9}$$

Since $\lambda \longrightarrow \infty$, both integrals at the right-hand side are 1-D stationary-phase integrals as seen in section A1. The only stationary point in the v_i integration domain is at $v_i = 0$; the phase term in the u_i integral is likewise stationary at $u_i = 0$ (provided that $v_i \approx 0$). Application of equation (A2) to the u_i integral in (A9) then gives

$$\int_{-\epsilon}^{+\epsilon} \mathrm{d}u_i \, \mathrm{e}^{\mathrm{i}\frac{\lambda}{2}\psi_{xxi}\left(u_i + \frac{\psi_{xyi}}{\psi_{xxi}}v_i\right)^2} = \mathrm{e}^{\pm\mathrm{i}\frac{\pi}{4}} \sqrt{\frac{2\pi}{\lambda|\psi_{xxi}|}}, \tag{A10}$$

where we have assumed $v_i \approx 0$ since this integral is to be evaluated near the stationary point of the v_i integral, and we have implicitly multiplied by 2 since equation (A2) is valid for a single stationary point located at one of the integration limits. Similarly,

$$\int_{-\delta}^{+\delta} \mathrm{d}v_i \, \mathrm{e}^{\mathrm{i}\frac{\lambda}{2}v_i^2\left(\psi_{yyi} - \frac{\psi_{xyi}^2}{\psi_{xxi}}\right)} = \mathrm{e}^{\pm\mathrm{i}\frac{\pi}{4}} \sqrt{\frac{2\pi}{\lambda\left|\psi_{yyi} - \frac{\psi_{xyi}^2}{\psi_{xxi}}\right|}}. \tag{A11}$$

Substituting equations (A10) and (A11) into (A9), we are left with the final formula

$$I(\lambda) \approx \frac{2\pi}{\lambda} \sum_i f(x_i, y_i) \mathrm{e}^{\mathrm{i}\left[\lambda\psi(x_i,y_i) \pm \frac{\pi}{4} \pm \frac{\pi}{4}\right]} \sqrt{\frac{1}{|\psi_{xxi}|\left|\psi_{yyi} - \frac{\psi_{xyi}^2}{\psi_{xxi}}\right|}}, \tag{A12}$$

valid for $\lambda \longrightarrow \infty$ and in the assumption that $\psi_{xxi} \neq 0$, $\psi_{yyi} - \frac{\psi_{xyi}^2}{\psi_{xxi}} \neq 0$. The signs of the $\pi/4$ terms in (A12) depend on those of ψ_{xxi} and $\psi_{yyi} - \psi_{xyi}^2/\psi_{xxi}$ (see section A1) [*Bender and Orszag*, 1978].

Appendix B: Fourier Transform Convention

Inverse and forward Fourier transformations are applied frequently throughout this study. We denote $\mathscr{F}$ and $\mathscr{F}^{-1}$ the forward and inverse Fourier transform operators, respectively. $\mathscr{F}$ and $\mathscr{F}^{-1}$ can be defined in various ways. We adopt here the following convention: for any function f,

$$f(\omega) = \mathscr{F}[f(t)] = \frac{1}{\sqrt{2\pi}} \int_{-\infty}^{+\infty} \mathrm{d}t \, f(t) \, \mathrm{e}^{-\mathrm{i}\omega t}, \tag{B1}$$

and consequently

$$f(t) = \mathscr{F}^{-1}[f(\omega)] = \frac{1}{\sqrt{2\pi}} \int_{-\infty}^{+\infty} \mathrm{d}\omega \, f(\omega) \, \mathrm{e}^{\mathrm{i}\omega t}, \tag{B2}$$

where we have chosen to simply specify the argument (time t or frequency ω, respectively) to distinguish a time domain function $f(t)$ from its Fourier transform $f(\omega)$.

Some properties of the Fourier transform are particularly useful in the context of ambient noise cross correlation. First of all, it follows from (B1) that the Fourier transform of the derivative of f with respect to t is

$$\mathscr{F}\left[\frac{\mathrm{d}f(t)}{\mathrm{d}t}\right] = \mathrm{i}\omega f(\omega). \tag{B3}$$

The Fourier transform of the integral of f is

$$\mathscr{F}\left[\int_{-\infty}^{t} f(\tau)\mathrm{d}\tau\right] = -\frac{\mathrm{i}}{\omega} f(\omega), \tag{B4}$$

provided that $f(t) \longrightarrow 0$ when $t \longrightarrow -\infty$.

Other useful properties of the Fourier transform concern even and odd functions. The Green's functions $G(t)$ we work with throughout this study (Appendix E) are real (in the time domain) and have the property $G(t) = 0$ if $t < 0$. Let us define the real, even function

$$G_e(t) = \frac{1}{2}G(t) + \frac{1}{2}G(-t), \tag{B5}$$

and the real, odd function

$$G_o(t) = \frac{1}{2}G(t) - \frac{1}{2}G(-t). \tag{B6}$$

The definitions (B5) and (B6) imply

$$G(t) = G_e(t) + G_o(t). \tag{B7}$$

It follows from (B1) that the Fourier transform of a real even function is even and purely real, while the Fourier transform of a real odd function is odd and purely imaginary. Then,

$$\Re\left[G(\omega)\right] = G_e(\omega) \tag{B8}$$

and

$$\Im\left[G(\omega)\right] = -\mathrm{i}G_o(\omega), \tag{B9}$$

where $\Re\left[G(\omega)\right]$ and $\Im\left[G(\omega)\right]$ denote the real and imaginary part of $G(\omega)$, respectively.

Appendix C: Bessel Functions

Bessel functions emerge frequently in noise literature, starting with the early works of, e.g., *Eckart* [1953], *Aki* [1957], and *Cox* [1973]. Their mathematical properties are described in detail by *Abramowitz and Stegun* [1964]. In seismic interferometry we are in practice only interested in zeroth-order Bessel functions of the first and second kind, denoted $J_0(\bullet)$, $Y_0(\bullet)$, respectively, which together with the Hankel functions $H_0^{(1)}(\bullet) = J_0(\bullet) + \mathrm{i}Y_0(\bullet)$ and $H_0^{(2)}(\bullet) = J_0(\bullet) - \mathrm{i}Y_0(\bullet)$ can be defined as the solutions of the zeroth-order Bessel equation

$$\frac{\mathrm{d}^2 f(x)}{\mathrm{d}x^2} + \frac{1}{x}\frac{\mathrm{d}f(x)}{\mathrm{d}x} + f(x) = 0 \tag{C1}$$

[*Abramowitz and Stegun*, 1964, equation (9.1.1)].

In our implementation we employ the far-field (large r) and/or high-frequency (large ω) approximations for $J_0(x)$, $Y_0(x)$, and $H_0^{(1)}(x)$, $H_0^{(2)}(x)$, namely,

$$J_0(x) \approx \sqrt{\frac{2}{\pi x}}\cos\left(x - \frac{\pi}{4}\right), \tag{C2}$$

$$Y_0(x) \approx \sqrt{\frac{2}{\pi x}}\sin\left(x - \frac{\pi}{4}\right), \tag{C3}$$

$$H_0^{(1)}(x) \approx \sqrt{\frac{2}{\pi x}} e^{i(x-\pi/4)}, \tag{C4}$$

$$H_0^{(2)}(x) \approx \sqrt{\frac{2}{\pi x}} e^{-i(x-\pi/4)} \tag{C5}$$

[*Abramowitz and Stegun*, 1964, equations (9.2.1)–(9.2.4)]. In practice, J_0 and Y_0 can roughly be thought of as "damped" sinusoidal functions, whose amplitude decays exponentially as their argument tends to infinity; at large x, J_0 approximates a cosine with a $\pi/4$ phase shift, and Y_0 approximates a sine with a $\pi/4$ phase shift.

Appendix D: Cancelation of Cross Terms

Throughout this study, simple analytical formulae for the cross correlation of an ambient wavefield are obtained neglecting the contribution of the so-called "cross terms," i.e., the receiver-receiver cross correlation of signal generated by a couple of different sources. We propose in the following a simple proof, similar to that of *Weemstra et al.* [2014], of the validity of this assumption.

The pressure due to an impulse emitted by source j at a random time t_j is given by equation (E21), after replacing $t - x/c$ with $t - t_j - x/c$ as argument of the Dirac function; in the frequency domain, this is equivalent to adding a phase anomaly $-i\omega t_j$ to the argument of the exponential in equation (E22). If N_S such sources are active during the time interval over which a cross correlation is conducted, the pressure p_i recorded at receiver i is a linear combination of the signals originating from these sources, i.e., in 3-D,

$$p_i(\omega) = \sum_{j=1}^{N_S} \frac{e^{-i\left(\frac{\omega r_{ij}}{c} + \omega t_j\right)}}{\sqrt{2\pi} 4\pi c r_{ij}}, \tag{D1}$$

where r_{ij} is the distance between receiver i and source j.

Cross correlating the signal recorded at $R1$ with that recorded at $R2$, we find

$$p_1(\omega) p_2^*(\omega) = \sum_{j=1}^{N_S} \sum_{k=1}^{N_S} \frac{e^{-i\frac{\omega}{c}(r_{1j} - r_{2k})}}{2\pi (4\pi c)^2 r_{1j} r_{2k}} e^{-i\omega(t_j - t_k)}, \tag{D2}$$

and the cross-term contribution can be isolated by separating $j \neq k$ terms (cross terms) from $j = k$ ones:

$$p_1(\omega) p_2^*(\omega) = \sum_{j=1}^{N_S} \frac{e^{-i\frac{\omega}{c}(r_{1j} - r_{2j})}}{r_{1j} r_{2j}} + \sum_{j=1}^{N_S} \sum_{j \neq k} \frac{e^{-i\frac{\omega}{c}(r_{1j} - r_{2k})}}{r_{1j} r_{2k}} e^{-i\omega(t_j - t_k)}. \tag{D3}$$

The first term at the right-hand side of equation (D3) is a sum of single-source cross correlations in 3-D (equation (6)). (The algebra is similar in 2-D (equation (7)), if the far-field approximation is applied.) Its average is given, e.g., by equations (8)–(10) above, which are obtained from (6) or (7) by neglecting the cross terms $j \neq k$ and replacing the sum over sources j with an integral over the area or volume occupied by the sources.

While $j \neq k$ terms in (D3) are nonnegligible, we next show that their contribution to the average of (D3) over a large set of sources is negligible. We make the assumptions that (i) at each realization, the values t_j change randomly and (ii) they are uniformly distributed between 0 and T_a, i.e., $0 < t_j < T_a$, where $T_a = 2\pi/\omega$. Let us introduce the phase $\phi_j = \omega t_j$, which is randomly distributed between 0 and 2π. The exponent $-i\omega(t_j - t_k)$ is accordingly replaced by $-i(\phi_j - \phi_k)$. In the process of averaging, impulses will be generated multiple times at each source location j, resulting in random phases ϕ_j. This is equivalent to requiring, as it is usually done in the literature, that noise sources be spatially and temporally uncorrelated [e.g., *Snieder*, 2004; *Roux et al.*, 2005]. To take into account the effects of random variations in phase, the $j \neq k$ term must consequently involve (besides the usual sum or integral over sources) an integral over all possible values (0 to 2π) of each source phase,

$$Av\left[\sum_{j=1}^{N_S} \sum_{j \neq k} \frac{e^{i\frac{\omega}{c}(r_{1j} - r_{2k})}}{2\pi\, r_{1j} r_{2k}} e^{i(\phi_j - \phi_k)}\right] = \frac{1}{(2\pi)^{N_S}} \int \int \ldots \int_0^{2\pi} \sum_{j=1}^{N_S} \sum_{j \neq k} \frac{e^{i\frac{\omega}{c}(r_{1j} - r_{2k})}}{2\pi\, r_{1j} r_{2k}} e^{i(\phi_j - \phi_k)} d\phi_1 d\phi_2 \ldots d\phi_{N_S}. \tag{D4}$$

All Integrals evaluate to zero because the integrands traverse a circle in the complex plane from 0 to 2π. Consequently, if cross correlations are averaged over sufficient realizations, the cross correlation in equation (D3) reduces to a sum of single-source cross correlations (noncross terms).

The averaging procedure we just described is often referred to as "ensemble-averaging" in ambient noise theory. This expression is borrowed from statistical mechanics: an "ensemble" is a set of states of a system, each described by the same set of microscopic forces and sharing some common macroscopic property. The ensemble concept then states that macroscopic observables can be calculated by performing averages over the states in the ensemble [*Tuckerman*, 1987]. In our case, one state consists of the same acoustic or elastic medium (its response to a given impulse is always the same) being illuminated by one or more randomly located sources with random phases: our ensemble average is the average over all possible combination of source locations and phases. Cross-correlating recordings associated with a single state (a unique combination of sources) yield many cross terms; we have just shown, however, that ensemble-averaging cross correlations over different states implies that these cross terms stack incoherently and hence become negligible. In the real world, the location and phase of noise sources (e.g., ocean microseisms) are not well known; the assumption is made that over time, a sufficiently diverse range of sources is sampled so that averaging the cross correlation over time (i.e., computing the cross correlation over a very long time window) is practically equivalent to ensemble-averaging.

Appendix E: Green's Functions of the Scalar Wave Equation (Homogeneous Lossless Media)

E1. Green's Problem as Homogeneous Equation

Following, e.g., *Roux et al.* [2005], *Sanchez-Sesma and Campillo* [2006], and *Harmon et al.* [2008], we call Green's function $G = G(\mathbf{x}, \mathbf{x}_S, t)$ the solution of

$$\nabla^2 G - \frac{1}{c^2}\frac{\partial^2 G}{\partial t^2} = 0 \tag{E1}$$

with initial conditions

$$G(\mathbf{x}, \mathbf{x}_S, 0) = 0, \tag{E2}$$

$$\frac{\partial G}{\partial t}(\mathbf{x}, \mathbf{x}_S, 0) = \delta(\mathbf{x} - \mathbf{x}_S), \tag{E3}$$

i.e., an impulsive source at $\mathbf{x}_S$. We are only interested in causal Green's functions, satisfying the radiation condition, i.e., vanishing at $t < 0$.

Once G is known, it can be used to solve rapidly more general initial value problems associated with (E1). Consider, for example,

$$\nabla^2 f - \frac{1}{c^2}\frac{\partial^2 f}{\partial t^2} = 0 \tag{E4}$$

with the more general initial conditions

$$f(\mathbf{x}, 0) = 0, \tag{E5}$$

$$\frac{\partial f}{\partial t}(\mathbf{x}, 0) = h(\mathbf{x}). \tag{E6}$$

It can be proved by direct substitution that if G solves (E1)–(E3) then

$$f(\mathbf{x}, t) = \int_{\mathbb{R}^d} \mathrm{d}^d\mathbf{x}\, G(\mathbf{x}, \mathbf{x}_S, t) h(\mathbf{x}) \tag{E7}$$

solves (E4)–(E6), with d denoting the number of dimensions: 2 or 3 in our case.

For the sake of simplicity, we shall set $\mathbf{x}_S = \mathbf{0}$ in the following. $G(\mathbf{x}, \mathbf{x}_S, t)$ can be recovered from $G(\mathbf{x}, 0, t)$ by translation of the reference frame.

E2. Solution in the Spatial Fourier Transform Domain

Equation (E1) can be solved via a spatial Fourier transform, i.e., by the *Ansatz*

$$G(\mathbf{x},t)=\frac{1}{(2\pi)^d}\int_{\mathbb{R}^d}\mathrm{d}^d\mathbf{k}\,G(\mathbf{k},t)\mathrm{e}^{\mathrm{i}\mathbf{k}\cdot\mathbf{x}}, \tag{E8}$$

which, substituted into (E1), gives

$$\frac{1}{c^2}\frac{\partial^2 G}{\partial t^2}(\mathbf{k},t)+k^2G(\mathbf{k},t)=0, \tag{E9}$$

with $k=|\mathbf{k}|$. Equation (E9) is solved by

$$G(\mathbf{k},t)=A(\mathbf{k})\cos(kct)+B(\mathbf{k})\sin(kct), \tag{E10}$$

where $A(\mathbf{k})$ and $B(\mathbf{k})$ must be determined by the initial conditions. Transforming (E2) and (E3) to $\mathbf{k}$ space, with

$$\delta(\mathbf{x})=\frac{1}{(2\pi)^d}\int_{\mathbb{R}^d}\mathrm{d}^d\mathbf{k}\,\mathrm{e}^{\mathrm{i}\mathbf{k}\cdot\mathbf{x}}, \tag{E11}$$

and replacing G in the resulting equations with its expression (E10), we find $A(\mathbf{k})=0$, $B(\mathbf{k})=\frac{1}{kc}$, and

$$G(\mathbf{k},t)=\frac{1}{kc}\sin(kct). \tag{E12}$$

Equation (E8) can now be used to determine $G(\mathbf{x},t)$ from its spatial Fourier transform $G(\mathbf{k},t)$, and the result differs importantly depending on d.

E3. Inverse Transform of the Solution to 2-D Space

Substituting (E12) into (E8) in the $d=2$ case,

$$G_{2D}(\mathbf{x},t)=\frac{1}{4\pi^2}\int_{-\infty}^{+\infty}\mathrm{d}k_1\int_{-\infty}^{+\infty}\mathrm{d}k_2\,\frac{\sin(kct)}{kc}\mathrm{e}^{\mathrm{i}\mathbf{k}\cdot\mathbf{x}}. \tag{E13}$$

We call ξ the angle between $\mathbf{k}$ and $\mathbf{x}$. It follows that $\mathbf{k}\cdot\mathbf{x}=kx\cos\xi$, with $x=|\mathbf{x}|$. For each $\mathbf{x}$ the integration can be conducted over k and ξ, using $\mathrm{d}k_1\mathrm{d}k_2=k\mathrm{d}k\mathrm{d}\xi$,

$$\begin{aligned}G_{2D}(\mathbf{x},t)&=\frac{1}{4\pi^2c}\int_0^{+\infty}\mathrm{d}k\sin(kct)\int_0^{2\pi}\mathrm{d}\xi\,\mathrm{e}^{\mathrm{i}kx\cos\xi}\\&=\frac{1}{2\pi^2c}\int_0^{+\infty}\mathrm{d}k\sin(kct)\int_0^{\pi}\mathrm{d}\xi\,\cos(kx\cos\xi)\\&=\frac{1}{2\pi c}\int_0^{+\infty}\mathrm{d}k\sin(kct)J_0(kx),\end{aligned} \tag{E14}$$

where we have used the symmetry properties of sine and cosine, and the integral form of the zeroth-order Bessel function of the first kind J_0 [*Abramowitz and Stegun*, 1964, equation (9.1.18)] (Appendix C). The remaining integral in (E14) is solved via equation (11.4.38) of *Abramowitz and Stegun* [1964], resulting in

$$G_{2D}(\mathbf{x},t)=\frac{1}{2\pi c^2}\frac{H\left(t-\frac{x}{c}\right)}{\sqrt{t^2-\frac{x^2}{c^2}}} \tag{E15}$$

[*Sanchez-Sesma and Campillo*, 2006; *Harmon et al.*, 2008], where H denotes the Heaviside function. Equation (E15), as well as other time domain formulae for the Green's function, is only physically meaningful for $t>0$. Dimensional analysis of (E15) shows that G_{2D} in this formulation has units of time over squared distance. The Fourier transform of $G_{2D}(\mathbf{x},t)$ is inferred from equation (9.1.24) of *Abramowitz and Stegun* [1964], after applying our definition (B1) to equation (E15):

$$\begin{aligned}G_{2D}(\mathbf{x},\omega)&=\frac{1}{\sqrt{8\pi^3}c^2}\int_{\frac{x}{c}}^{\infty}\mathrm{d}t\frac{\mathrm{e}^{-\mathrm{i}\omega t}}{\sqrt{t^2-\frac{x^2}{c^2}}}\\&=\frac{1}{\sqrt{8\pi^3}c^2}\int_1^{\infty}\mathrm{d}t'\frac{\mathrm{e}^{-\mathrm{i}\frac{\omega x}{c}t'}}{\sqrt{t'^2-1}}\\&=-\frac{1}{4\sqrt{2\pi}c^2}\left[Y_0\left(\frac{\omega x}{c}\right)+\mathrm{i}J_0\left(\frac{\omega x}{c}\right)\right]\\&=\frac{1}{4\mathrm{i}\sqrt{2\pi}c^2}H_0^{(2)}\left(\frac{\omega x}{c}\right)\end{aligned} \tag{E16}$$

[*Sanchez-Sesma and Campillo*, 2006; *Harmon et al.*, 2008], where Y_0 and $H_0^{(2)}$ denote the zeroth-order Bessel function of the second kind and the zeroth-order Hankel function of the second kind [*Abramowitz and Stegun*, 1964] (Appendix C). Based upon the far-field/high-frequency asymptotic form (C5) of $H_0^{(2)}$, we can also write

$$G_{2D}(\mathbf{x},\omega) \approx \frac{1}{4\mathrm{i}\pi c^{3/2}} \frac{\mathrm{e}^{-\mathrm{i}\left(\frac{\omega x}{c}-\frac{\pi}{4}\right)}}{\sqrt{\omega x}}, \tag{E17}$$

which is analogous to equation (14) of *Snieder* [2004].

Equation (9.1.24) of *Abramowitz and Stegun* [1964] is only valid for positive frequency $\omega > 0$, and so is, as a consequence, our relation (E16). We know, however, that $G_{2D}(\mathbf{x},t)$ is a real-valued function: the relationship $G_{2D}(\mathbf{x},\omega) = G^*_{2D}(\mathbf{x},-\omega)$ then holds and allows us to define G_{2D} in the entire frequency domain.

E4. Inverse Transform of the Solution to 3-D Space

We now substitute (E12) into the 3-D version of (E8) and find

$$G_{3D}(\mathbf{x},t) = \frac{1}{8\pi^3} \int_{-\infty}^{+\infty} \mathrm{d}k_1 \int_{-\infty}^{+\infty} \mathrm{d}k_2 \int_{-\infty}^{+\infty} \mathrm{d}k_3 \, \frac{\sin(kct)}{kc} \mathrm{e}^{\mathrm{i}\mathbf{k}\cdot\mathbf{x}}. \tag{E18}$$

The integral in (E18) is simplified by switching from k_1, k_2, k_3 to spherical coordinates k, ξ, χ, with the $\xi = 0$ direction coinciding with that of $\mathbf{x}$. Then $\mathrm{d}k_1\mathrm{d}k_2\mathrm{d}k_3 = -k^2\mathrm{d}k\mathrm{d}\chi\mathrm{d}(\cos\xi)$, $\mathbf{k}\cdot\mathbf{x} = kx\cos\xi$, and

$$\begin{aligned} G_{3D}(\mathbf{x},t) &= -\frac{1}{8\pi^3} \int_0^{+\infty} \mathrm{d}k \, \frac{k\sin(kct)}{c} \int_0^{2\pi} \mathrm{d}\chi \int_1^{-1} \mathrm{d}(\cos\xi)\, \mathrm{e}^{\mathrm{i}kx\cos\xi} \\ &= \frac{1}{2\pi^2 cx} \int_0^{+\infty} \mathrm{d}k \, \sin(kct)\sin(kx). \end{aligned} \tag{E19}$$

The k integral in (E19) is solved via the equality $\sin\alpha\sin\beta = \frac{1}{2}[\cos(\alpha-\beta) - \cos(\alpha+\beta)]$, which gives

$$\begin{aligned} G_{3D}(\mathbf{x},t) &= \frac{1}{4\pi^2 cx} \int_0^{+\infty} \mathrm{d}k \, \{\cos[k(ct-x)] - \cos[k(ct+x)]\} \\ &= \frac{1}{4\pi^2 cx} \lim_{z\to\infty} \left\{ \left[\frac{\sin[k(ct-x)]}{ct-x}\right]_{k=0}^{k=z} - \left[\frac{\sin[k(ct+x)]}{ct+x}\right]_{k=0}^{k=z} \right\} \\ &= \frac{1}{4\pi cx} \left[\delta\left(t-\frac{x}{c}\right) - \delta\left(t+\frac{x}{c}\right)\right], \end{aligned} \tag{E20}$$

where we have used the property of the Dirac δ function that $\delta(x) = \frac{1}{\pi}\lim_{z\to\infty}\frac{\sin(zx)}{x}$ [e.g., *Weisstein*, 1999–2013]. In our formulation both t and x are positive so that $\delta\left(t+\frac{x}{c}\right) = 0$, and we are left with

$$G_{3D}(\mathbf{x},t) = \frac{1}{4\pi c} \frac{\delta\left(t-\frac{x}{c}\right)}{x} \tag{E21}$$

[e.g., *Aki and Richards*, 2002, chap. 4]. Notice that since the dimension of the Dirac δ is the inverse of that of its argument, that of G_{3D} is one over squared distance. According to (B1), $\mathscr{F}[\delta(t-t_0)] = \frac{1}{\sqrt{2\pi}}\mathrm{e}^{-\mathrm{i}\omega t_0}$, and consequently,

$$G_{3D}(\mathbf{x},\omega) = \frac{1}{\sqrt{2\pi}} \frac{1}{4\pi c} \frac{\mathrm{e}^{-\mathrm{i}\frac{\omega x}{c}}}{x}. \tag{E22}$$

E5. Green's Problem as Inhomogeneous Equation

The Green's problem is also often written as equation (1) plus an impulsive forcing term, i.e.,

$$\nabla^2 g - \frac{1}{c^2}\frac{\partial^2 g}{\partial t^2} = \delta(\mathbf{x})\delta(t), \tag{E23}$$

with initial conditions

$$g(\mathbf{x},0) = 0, \tag{E24}$$

$$\frac{\partial g}{\partial t}(\mathbf{x},0) = 0. \tag{E25}$$

The solution g to this problem is related to the solution G of (E1)–(E3), namely,

$$g(\mathbf{x}, t) = \int_0^t \mathrm{d}s\, G(\mathbf{x}, t - s). \tag{E26}$$

We demonstrate that (E26) solves (E23)–(E25) via Duhamel's principle [e.g., *Hildebrand*, 1976; *Strauss*, 2008]: let us consider the more general case

$$\nabla^2 u - \frac{1}{c^2}\frac{\partial^2 u}{\partial t^2} = h(\mathbf{x}, t), \tag{E27}$$

$$u(\mathbf{x}, 0) = 0, \tag{E28}$$

$$\frac{\partial u}{\partial t}(\mathbf{x}, 0) = 0, \tag{E29}$$

with h an arbitrary forcing term. Suppose that a solution $v(\mathbf{x}, t)$ to the following homogeneous problem, closely related to (E27)–(E29), can be found:

$$\nabla^2 v - \frac{1}{c^2}\frac{\partial^2 v}{\partial t^2} = 0, \tag{E30}$$

$$v(\mathbf{x}, 0; s) = 0, \tag{E31}$$

$$\frac{\partial v}{\partial t}(\mathbf{x}, 0; s) = h(\mathbf{x}, s). \tag{E32}$$

(In practice, a solution of equation (E30) that satisfies the initial condition (E32) must be determined for any possible value of the parameter s in (E32); s replaces t in the expression of h first encountered in (E27).) Then, the following relation between u and v holds

$$u(\mathbf{x}, t) = \int_0^t \mathrm{d}s\, v(\mathbf{x}, t - s; s). \tag{E33}$$

One can verify that (E33) solves (E30)–(E32) by direct substitution, applying Leibniz's rule for differentiating under the integral sign. Equation (E26) is a particular case of (E33).

Result (E33) can also be combined with (E7) to write the solution of the general inhomogeneous problem (E27) in terms of the Green's function G (e.g., G_{2D} or G_{3D}). Replacing v in equation (E33) with expression (E7),

$$u(\mathbf{x}, t) = \int_0^t \mathrm{d}s \int_{\mathbb{R}_d} \mathrm{d}^d\mathbf{x}\, G(\mathbf{x}, \mathbf{x}_s, t - s; s) h(\mathbf{x}, s) \qquad (d = 2, 3). \tag{E34}$$

Acknowledgments
This study greatly benefitted from our discussions with M. Campillo, L. Campos-Venuti, A. Colombi, A. Curtis, J. de Rosny, J. P. Montagner, P. Poli, R. Snieder, P. Roux, J. Verbeke, K. Wapenaar, and four anonymous reviewers. Data and software used to produce the results of this paper can be obtained by e-mailing the first author: lapo.boschi@upmc.fr.

The Editor on this paper was Mark Moldwin. He thanks four anonymous reviewers for their assistance in reviewing this manuscript.

References

Abramowitz, M., and I. A. Stegun (1964), *Handbook of Mathematical Functions*, Natl. Bur. of Stand.–Appl. Math. Ser., Washington, D. C.
Aki, K. (1957), Space and time spectra of stationary waves with special reference to microtremors, *Bull. Earthquake Res. Inst. Univ. Tokyo*, *35*, 415–456.
Aki, K., and P. G. Richards (2002), *Quantitative Seismology*, 2nd ed., Univ. Science Books, Sausalito, Calif.
Bender, C. M., and S. A. Orszag (1978), *Advanced Mathematical Methods for Scientists and Engineers*, McGraw-Hill, New York.
Bensen, G. D., M. H. Ritzwoller, M. P. Barmin, A. L. Levshin, F. Lin, M. P. Moschetti, N. M. Shapiro, and Y. Yang (2007), Processing seismic ambient noise data to obtain reliable broad-band surface wave dispersion measurements, *Geophys. J. Int.*, *169*, 1239–1260, doi:10.1111/j.1365-246X.2007.03374.x.
Boschi, L., C. Weemstra, J. Verbeke, G. Ekström, A. Zunino, and D. Giardini (2013), On measuring surface wave phase velocity from station-station cross-correlation of ambient signal, *Geophys. J. Int.*, *192*, 346–358, doi:10.1093/gji/ggs023.
Brenguier, F., D. Clarke, Y. Aoki, N. M. Shapiro, M. Campillo, and V. Ferrazzini (2011), Monitoring volcanoes using seismic noise correlations, *C. R. Geosci.*, *343*, 633–638.
Campillo, M., and A. Paul (2003), Long-range correlations in the diffuse seismic coda, *Science*, *299*, 547–549.

Campillo, M., and P. Roux (2014), Seismic imaging and monitoring with ambient noise correlations, in *Treatise of Geophysics*, vol. 1, edited by B. Romanowicz and A. M. Dziewonski, Elsevier, Amsterdam.
Claerbout, J. F. (1968), Synthesis of a layered medium from its acoustic transmission response, *Geophysics*, *33*, 264–269.
Colombi, A., L. Boschi, P. Roux, and M. Campillo (2014), Green's function retrieval through cross-correlations in a two-dimensional complex reverberating medium, *J. Acoust. Soc. Am.*, *135*, 1034–1043, doi:10.1121/1.4864485.
Cooley, J. W., and J. W. Tukey (1965), An algorithm for the machine calculation of complex Fourier series, *Math. Comput.*, *19*, 297–301.
Corciulo, M., P. Roux, M. Campillo, and D. Dubucq (2012), Instantaneous phase variation for seismic velocity monitoring from ambient noise at the exploration scale, *Geophysics*, *77*, Q37–Q44, doi:10.1190/geo2011–0363.1.
Cox, H. (1973), Spatial correlation in arbitrary noise fields with application to ambient sea noise, *J. Acoust. Soc. Am.*, *54*, 1289–1301.
Curtis, A., P. Gerstoft, H. Sato, R. Snieder, and K. Wapenaar (2006), Interferometry—Turning noise into signal, *The Leading Edge*, *25*, 1082–1092.
De Ridder, S., and J. Dellinger (2011), Ambient seismic noise eikonal tomography for near-surface imaging at Valhall, *The Leading Edge*, *30*, 506–512, doi:10.1190/1.3589108.
De Ridder, S. A. L., B. L. Biondi, and R. G. Clapp (2014), Time-lapse seismic noise correlation tomography at Valhall, *Geophys. Res. Lett.*, *41*, 6116–6122, doi:10.1002/2014GL061156.1.
Derode, A., E. Larose, M. Campillo, and M. Fink (2003), How to estimate the Green's function of a heterogeneous medium between two passive sensors? Application to acoustic waves, *Appl. Phys. Lett.*, *83*, 3054–3056, doi:10.1063/1.1617373.
Duvall, T. L., S. M. Jefferies, J. W. Harvey, and M. A. Pomerantz (1993), Time-distance helioseismology, *Nature*, *362*, 430–432.
Eckart, C. (1953), The theory of noise in continuous media, *J. Acoust. Soc. Am.*, *25*, 195–199.
Ekström, G. (2014), Love and Rayleigh phase-velocity maps, 5–40 s, of the western and central USA from USArray data, *Earth Planet. Sci. Lett.*, *402*, 42–49.
Ekström, G., G. A. Abers, and S. C. Webb (2009), Determination of surface-wave phase velocities across USArray from noise and Aki's spectral formulation, *Geophys. Res. Lett.*, *36*, L18301, doi:10.1029/2009GL039131.
Fink, M. (1999), Time-reversed acoustics, *Sci. Am.*, *281*, 91–97.
Fink, M. (2006), Time-reversal acoustics in complex environments, *Geophysics*, *71*, SI151–SI164, doi:10.1190/1.2215356.
Fleury, C., R. Snieder, and K. Larner (2010), General representation theorem for perturbed media and application to green's function retrieval for scattering problems, *Geophys. J. Int.*, *183*, 1648–1662.
Gorbatov, A., E. Saygin, and B. L. N. Kennett (2013), Crustal properties from seismic station autocorrelograms, *Geophys. J. Int.*, *192*, 861–870, doi:10.1093/gji/ggs064.
Gouedard, P., et al. (2008), Cross-correlation of random fields: Mathematical approach and applications, *Geophys. Prospect.*, *56*, 375–393.
Groenenboom, J., and R. Snieder (1995), Attenuation, dispersion, and anisotropy by multiple scattering of transmitted waves through distribution of scattering, *J. Acoust. Soc. Am.*, *98*, 3482–3492.
Gualtieri, L., E. Stutzmann, Y. Capdeville, F. Ardhuin, M. Schimmel, A. Mangeney, and A. Morelli (2013), Modelling secondary microseismic noise by normal mode summation, *Geophys. J. Int.*, *193*, 1732–1745, doi:10.1093/gji/ggt090.
Halliday, D., and A. Curtis (2008), Seismic interferometry, surface waves and source distribution, *Geophys. J. Int.*, *175*, 1067–1087, doi:10.1111/j.1365-246X.2008.03918.x.
Haney, M. M. (2009), Infrasonic ambient noise interferometry from correlations of microbaroms, *Geophys. Res. Lett.*, *36*, L19808, doi:10.1029/2009GL040179.
Harmon, N., P. Gerstoft, C. A. Rychert, G. A. Abers, M. S. de la Cruz, and K. M. Fischer (2008), Phase velocities from seismic noise using beamforming and cross correlation in Costa Rica and Nicaragua, *Geophys. Res. Lett.*, *35*, L19303, doi:10.1029/2008GL035387.
Hasselmann, K. (1963), A statistical analysis of the generation of microseisms, *Rev. Geophys.*, *1*, 177–210, doi:10.1029/RG001i002p00177.
Hildebrand, F. B. (1976), *Advanced Calculus for Applications*, 2nd ed., Prentice-Hall, Englewood Cliffs, N. J.
Hillers, G., N. Graham, M. Campillo, S. Kedar, M. Landes, and N. Shapiro (2012), Global oceanic microseism sources as seen by seismic arrays and predicted by wave action models, *Geochem. Geophys. Geosyst.*, *13*, Q01021, doi:10.1029/2011GC003875.
Ito, Y., and K. Shiomi (2012), Seismic scatterers within subducting slab revealed from ambient noise autocorrelation, *Geophys. Res. Lett.*, *39*, L19303, doi:10.1029/2012GL053321.
Kedar, S., M. Longuet-Higgins, F. Webb, N. Graham, R. Clayton, and C. Jones (2008), The origin of deep ocean microseisms in the North Atlantic Ocean, *Proc. R. Soc. London, Ser. A*, *464*, 777–793, doi:10.1098/rspa.2007.0277.
Kinsler, L. E., A. R. Frey, A. B. Coppens, and J. V. Sanders (1999), *Fundamentals of Acoustics*, 4th ed., Wiley, Hoboken, N. J.
Kohler, M. D., T. H. Heaton, and S. C. Bradford (2007), Propagating waves in the steel, moment-frame factor building recorded during earthquakes, *Bull. Seismol. Soc. Am.*, *97*, 1334–1345, doi:10.1785/0120060148.
Larose, E., L. Margerin, A. Derode, B. van Tiggelen, M. Campillo, N. M. Shapiro, A. Paul, L. Stehly, and M. Tanter (2006), Correlation of random wave fields: An interdisciplinary review, *Geophysics*, *71*, SI11–SI21.
Lobkis, O. I., and R. L. Weaver (2001), On the emergence of the Green's function in the correlations of a diffuse field, *J. Acoust. Soc. Am.*, *110*, 3011–3016, doi:10.1121/1.1417528.
Longuet-Higgins, M. S. (1950), A theory of the origin of microseisms, *Philos. Trans. R. Soc. London, Ser. A*, *243*, 1–35.
Mainsant, G., E. Larose, C. Brönnimann, D. Jongmans, C. Michoud, and M. Jaboyedoff (2012), Ambient seismic noise monitoring of a clay landslide: Toward failure prediction, *J. Geophys. Res.*, *117*, F01030, doi:10.1029/2011JF002159.
Malcolm, A. E., J. A. Scales, and B. A. van Tiggelen (2004), Extracting the green function from diffuse, equipartitioned waves, *Phys. Rev. E*, *70*, 015601, doi:10.1103/PhysRevE.70.015601.
Marston, P. L. (2001), Generalized optical theorem for scatterers having inversion symmetry: Applications to acoustic backscattering, *J. Acoust. Soc. Am.*, *109*, 1291–1295.
Mikesell, T. D., K. van Wijk, T. E. Blum, R. Snieder, and H. Sato (2012), Analyzing the coda from correlating scattered surface waves, *J. Acoust. Soc. Am.*, *131*, EL275–EL281, doi:10.1121/1.3687427.
Morse, P. K., and K. U. Ingard (1986), *Theoretical Acoustics*, Princeton Univ. Press, Princeton, N. J.
Mulargia, F. (2012), The seismic noise wavefield is not diffuse, *J. Acoust. Soc. Am.*, *131*, 2853–2858, doi:10.1121/1.3689551.
Nakahara, H. (2006), A systematic study of theoretical relations between spatial correlation and Green's function in one-, two- and three-dimensional random scalar wavefields, *Geophys. J. Int.*, *167*, 1097–1105, doi:10.1111/j.1365-246X.2006.03170.x.
Newton, R. G. (2002), *Scattering Theory of Waves and Particles*, Dover, Mineola, New York.
Nishida, K. (2013), Global propagation of body waves revealed by cross-correlation analysis of seismic hum, *Geophys. Res. Lett.*, *40*, 1691–1696, doi:10.1002/grl.50269.
Poli, P., H. A. Pedersen, M. Campillo, and POLENET/LAPNET Working Group (2012a), Emergence of body waves from cross-correlation of short period seismic noise, *Geophys. J. Int.*, *188*, 549–558, doi:10.1111/j.1365-246X.2011.05271.x.

Poli, P., H. A. Pedersen, M. Campillo, and POLENET/LAPNET Working Group (2012b), Body-wave imaging of Earth's mantle discontinuities from ambient seismic noise, *Science*, *338*, 1063–1065, doi:10.1126/science.1228194.
Ravasi, M., and A. Curtis (2013), Nonlinear scattering based imaging in elastic media: Theory, theorems, and imaging conditions, *Geophysics*, *78*, S137–S155, doi:10.1190/GEO2012-0286.1.
Ritzwoller, M. (2014), Ambient noise seismic imaging, in *McGraw Hill Year Book on Science and Technology*, pp. 1–13, McGraw-Hill, New York.
Roux, P., K. Sabra, W. Kuperman, and A. Roux (2005), Ambient noise cross correlation in free space: Theoretical approach, *J. Acoust. Soc. Am.*, *117*, 79–84, doi:10.1121/1.1830673.
Ruigrok, E., X. Campman, and K. Wapenaar (2011), Extraction of P-wave reflections from microseisms, *C. R. Geosci.*, *343*, 512–525.
Sanchez-Sesma, F. J., and M. Campillo (2006), Retrieval of the Green's function from cross correlation: The canonical elastic problem, *Bull. Seismol. Soc. Am.*, *96*, 1182–1191, doi:10.1785/0120050181.
Sato, H. (2010), Retrieval of Green's function having coda waves from the cross-correlation function in a scattering medium illuminated by a randomly homogeneous distribution of noise sources on the basis of the first-order Born approximation, *Geophys. J. Int.*, *180*, 759–764, doi:10.1111/j.1365–246X.2009.04432.x.
Shapiro, N. M., M. Campillo, L. Stehly, and M. H. Ritzwoller (2005), High-resolution surface-wave tomography from ambient seismic noise, *Science*, *307*, 1615–1618.
Smith, S. W. (2011), *The Scientist and Engineer's Guide to Digital Signal Processing*, Calif. Tech. Publ. [Available at http://www.dspguide.com/.]
Snieder, R. (1986), 3D linearized scattering of surface waves and a formalism for surface wave holography, *Geophys. J. R. Astron. Soc.*, *84*, 581–605.
Snieder, R. (2004), Extracting the Green's function from the correlation of coda waves: A derivation based on stationary phase, *Phys. Rev. E*, *69*, 046610, doi:10.1103/PhysRevE.69.046610.
Snieder, R. (2007), Extracting the Green's function of attenuating heterogeneous acoustic media from uncorrelated waves, *J. Acoust. Soc. Am.*, *121*, 2637–2643, doi:10.1121/1.2713673.
Snieder, R., and E. Larose (2013), Extracting Earth's elastic wave response from noise measurements, *Annu. Rev. Earth Planet. Sci.*, *41*, 183–206, doi:10.1146/annurev-earth-050212-123936.
Snieder, R., and E. Şafak (2006), Extracting the building response using seismic interferometry: Theory and application to the Millikan Library in Pasadena, California, *Bull. Seismol. Soc. Am.*, *96*, 586–598, doi:10.1785/0120050109.
Snieder, R., K. van Wijk, M. Haney, and R. Calvert (2008), Cancellation of spurious arrivals in Green's function extraction and the generalized optical theorem, *Phys. Rev. E*, *78*, 036606, doi:10.1103/PhysRevE.78.036606.
Snieder, R., Y. Fan, E. Slob, and K. Wapenaar (2010), Equipartitioning is not sufficient for Green's function extraction, *Earthquake Sci.*, *23*, 403–415, doi:10.1007/s11589-010-0739-1.
Stehly, L. (2007), Tomography using correlations of seismic ambient noise, thesis, Univ. Joseph Fourier, Grenoble, France.
Stehly, L., M. Campillo, and N. M. Shapiro (2006), A study of the seismic noise from its long-range correlation properties, *J. Geophys. Res.*, *111*, B10306, doi:10.1029/2005JB004237.
Strauss, W. A. (2008), *Partial Differential Equations*, John Wiley, Hoboken, N. J.
Tanimoto, T. (1990), Modelling curved surface wave paths: Membrane surface wave synthetics, *Geophys. J. Int.*, *102*, 89–100.
Traer, J., and P. Gerstoft (2014), A unified theory of microseisms and hum, *J. Geophys. Res. Solid Earth*, *119*, 3317–3339, doi:10.1002/2013JB010504.
Tromp, J., and F. Dahlen (1993), Variational principles for surface wave propagation on a laterally heterogeneous Earth–III. Potential representation, *Geophys. J. Int.*, *112*, 195–209.
Tsai, V. C (2009), On establishing the accuracy of noise tomography travel-time measurements in a realistic medium, *Geophys. J. Int.*, *178*, 1555–1564, doi:10.1111/j.1365-246X.2009.04239.x.
Tuckerman, M. E. (1987), *Statistical Mechanics: Theory and Molecular Simulation*, Oxford Univ. Press, Oxford, U. K.
Udías, A. (1999), *Principles of Seismology*, Cambridge Univ. Press, Cambridge, U. K.
van Manen, D.-J., J. O. A. Robertsson, and A. Curtis (2005), Modeling of wave propagation in inhomogeneous media, *Phys. Rev. Lett.*, *94*, 164301, doi:10.1103/PhysRevLett.94.164301.
Wapenaar, K. (2004), Retrieving the elastodynamic Green's function of an arbitrary inhomogeneous medium by cross correlation, *Phys. Rev. Lett.*, *93*, 254301, doi:10.1103/PhysRevLett.93.254301.
Wapenaar, K., and J. Fokkema (2006), Green's function representations for seismic interferometry, *Geophysics*, *71*, SI33–SI46, doi:10.1190/1.2213955.
Wapenaar, K., J. Fokkema, and R. Snieder (2005), Retrieving the Green's function in an open system by cross correlation: A comparison of approaches, *J. Acoust. Soc. Am.*, *118*, 2783–2786, doi:10.1121/1.2046847.
Wapenaar, K., E. Slob, and R. Snieder (2006), Unified Green's function retrieval by seismic interferometry, *Phys. Rev. Lett.*, *97*, 234301.
Wapenaar, K., E. Slob, R. Snieder, and A. Curtis (2010a), Tutorial on seismic interferometry: Part 2—Underlying theory and new advances, *Geophysics*, *75*, A211–A227, doi:10.1190/1.3463440.
Wapenaar, K., D. Draganov, R. Snieder, X. Campman, and A. Verdel (2010b), Tutorial on seismic interferometry: Part 1—Basic principles and applications, *Geophysics*, *75*, A195–A209, doi:10.1190/1.3457445.
Weaver, R., B. Froment, and M. Campillo (2009), On the correlation of non-isotropically distributed ballistic scalar diffuse waves, *J. Acoust. Soc. Am.*, *126*, 1817–1826, doi:10.1121/1.3203359.
Weaver, R. L., and O. I. Lobkis (2002), On the emergence of the Green's function in the correlations of a diffuse field: Pulse-echo using thermal phonons, *Ultrasonics*, *40*, 435–439.
Weaver, R. L., and O. I. Lobkis (2004), Diffuse fields in open systems and the emergence of the Green's function, *J. Acoust. Soc. Am.*, *116*, 2731–2734.
Weemstra, C., L. Boschi, A. Goertz, and B. Artman (2013), Seismic attenuation from recordings of ambient noise, *Geophysics*, *78*, Q1–Q14, doi:10.1190/geo2012-0132.1.
Weemstra, C., W. Westra, R. Snieder, and L. Boschi (2014), On estimating attenuation from the amplitude of the spectrally whitened ambient seismic field, *Geophys. J. Int.*, *197*, 1770–1788, doi:10.1093/gji/ggu088.
Wegler, U., and C. Sens-Schonfelder (2007), Fault zone monitoring with passive image interferometry, *Geophys. J. Int.*, *168*, 1029–1033.
Weisstein, E. W. (1999–2013), Delta Function, From MathWorld—A Wolfram Web Resource. [Available at http://mathworld.wolfram.com/DeltaFunction.html.]
Wong, R. (1986), *Asymptotic Approximations of Integrals*, Soc. for Ind. and Appl. Math., Philadephia, Pa.
Woodard, M. F. (1997), Implications of localized, acoustic absorption for heliotomographic analysis of sunspots, *Astrophys. J.*, *485*, 890–894.